NTNU
Norwegian University of
Science and Technology

Mucins: Galectin 3 interactions measured by atomic force microscopy

Carbohydrate antigens in human health and disease

Ragna Emilie Bugge

Chemical Engineering and Biotechnology
Submission date: June 2017
Supervisor: Marit Sletmoen, IBT

Norwegian University of Science and Technology
Department of Biotechnology and Food Science

Abstract

Galectins are a family of widely distributed sugar-binding proteins characterized by a specificity for β-galactosides. These lectins are assumed to be involved in diverse biological phenomena critical for multicellular organisms, and despite the recognized importance of this, there is a lack of information concerning the mechanisms underlying their assumed functions.
An improved understanding of the physiological roles of the different members of the galectin family requires an improved understanding of their sugar-binding specify. The Galectin 3 (Gal3) is known to bind the human Mucin1 with T glycans (MUC1-T), but we have preliminary data from an unpublished study at King's Collage London, indicating that it might bind MUC1 with ST glycans (MUC1-ST) as well. Gal3 interaction with MUC1-ST, MUC1-T, MUC1 with Tn glycans (MUC1-Tn), and MUC1 with no glycans (MUC1-Naked) were investigated by atomic force microscopy (AFM). Interaction events were observed between MUC1-ST and Gal3, similar to those between MUC1-T and Gal3. These new findings could have implications of the understanding of the role of Gal3 and MUC1 for cancer progression and treatment. However, since some interaction events were observed also for the MUC1-Tn interaction with Gal3 and the MUC1-Naked interaction with Gal3, it can at this stage not be ruled out that the observed interactions between MUC1-ST and Gal3 are non-specific.
Interactions between MUC1-ST and Gal3 were observed at a frequency of 20.8% ±0.6, while interactions between MUC1-T and Gal3 were observed at a frequency of 12% ±6. Interactions between Gal3 and MUC1-Tn were observed at a frequency of 5% ±1, while interactions between Gal3 and MUC-Naked were observed at a frequency of 10% ±3. MUC1-Tn and MUC1-Naked were both used as negative controls.
Further it was showed that a dynamic force spectroscopic analysis suggested an energy landscape for interaction between Gal3 and MUC1-ST, with binding strengths from 40 pN to 80 pN at a loading rate interval of 1128-12512 pN/s. By utilizing the Bell-Evans model, a single energy barrier was identified at x_β=0.21 nm, and a mean dissociation rate was estimated to be $\overline{k_{off}}$=8 s^{-1}, corresponding to a lifetime of τ_0=0.125 s. Similar parameters were also obtained from interactions between Gal3 and MUC1-T, which exhibited an energy landscape with strengths ranging from 33 pN to 80 pN at a loading

rate interval of 787-6962 pN/s. Here, a single energy barrier was identified at x_β=0.20 nm, and a mean dissociation rate was estimated to be $\overline{k_{off}}$=4 s^{-1}, corresponding to a lifetime of τ_0=0.25 s.

Comparison between the data obtained from AFM and data obtained from optical tweezer (OT) in a parallel experiment conducted by another master student, Øystein Haug, revealed a similar linear relationship between most probable rupture force and loading rate for interactions between Gal3 and MUC1. Based on this, a new x_β was estimated to be 0.15 nm.

Implementation of new models for dynamic force spectroscopy analysis would provide more precise estimate of the parameters. Studies on a cellular level could confirm or reject the specificity of the interaction between MUC1-ST and Gal3, and the intracellular mechanisms they might set off.

Sammendrag

Galektiner er en familie av sukkerbindende proteiner kjennetegnet av sin spesifisitet for β-galactosider. Det er antatt at disse lektinene er involvert i ulike biologiske fenomener som er kritiske for multicellulære organismer, og til tross for denne anerkjente betydningen, mangler det fortsatt informasjon om mekanismene som ligger til grunn for deres antatte funksjoner.
En bedre forståelse av de fysiologiske funksjonene til de forskjellige medlemmene av galektinfamilien krever en bedre forståelse av deres sukkerbindingsspesifisitet. Galektin 3 (Gal3) er kjent for å binde human Mucin 1 med T glykaner (MUC1-T), men vi har foreløpige data fra en upublisert studie ved King's Collage London som indikerer at det kan binde human mucin med ST glykaner (MUC1-ST) også. Interaksjoner mellom Gal3 og mucinene MUC1-ST, MUC1-T, MUC1 med Tn glykaner (MUC1Tn), og MUC1 uten glykaner (MUC1-Naked) ble undersøkt med atomic force microscopy (AFM). Interaksjonshendelser som ble observert mellom MUC1-ST og Gal3, lignet de mellom MUC1-T og Gal3. Disse nye funnene kan ha konsekvenser for forståelsen av funksjonene til Gal3 og MUC1 for kreftprogresjon og behandling. Da noen interaksjonshendelser også ble observert for MUC1-Tn med Gal3 og MUC1-Naked med Gal3, kan vi i denne fasen ikke utelukkes at de observerte interaksjonene mellom MUC1-ST og Gal3 er uspesifikk.
Interaksjonshendelser mellom MUC1-ST og Gal3 ble observert med en frekvens på 20.8% ±0.6, mens interaksjoner mellom MUC1-T og Gal3 oppsto med en frekvens på 12& ±6. Interaksjonshendelser mellom Gal3 og MUC1-Tn ble observert med en frekvens på 5% ±1, mens interaksjoner mellom Gal3 og MUC1-Naked ble observert med en frekvens på 10% ±3. MUC1-Tn of MUC1-Naked ble begge brukt som negative kontroller.
Videre ble det skissert et energilandskap for interaksjonene mellom Gal3 of MUC1-ST med bindingstyrker fra 40 till 80 pN ved en belastningsrate fra 1128 pN/s til 12512 pN/s. Ved bruk av Bell-Evans modellen ble det identifisert en barriere ved x_β=0.21nm med en gjennomsnittlig dissosiasjonsrate, $\overline{k_{off}}$, på 8 s^{-1}, som tilsvarer en levetid, τ_0, på 0.125 s. Lignende parametere ble også beregnet for interaksjoner mellom Gal3 og MUC1-T som hadde et energilandskap med bindingsstyrker fra 33 pN til 80 pN ved en

belastningsrate fra 787 pN/s til 6962 pN/s. Her ble en energibarriere identifisert ved x_β=0.20 nm, $\overline{k_{off}}$ ble estimert til å være 4 s^{-1}, som tilsvarer en levetid, τ_0, på 0.52 s.
En sammenligning mellom data tatt opp ved hjelp av AFM og data tatt opp med optisk pinsett (OT) i et parallelt eksperiment utførte av en annen masterstudent, Øystein Haug, viste at disse dataene hadde et lignende lineært forhold mellom mest sannsynlig bruddstyrke og logaritmen av belastningsraten. Dette gav mulighet til å beregne en ny x_β til 0.15nm.
Implementering av nye modeller for dynamisk kraftspektroskopianalyse, vil kunne gi en mer nøyaktig estimering av parameterne. Studier på et cellulært nivå kan bekrefte eller avkrefte spesifikke interaksjonen mellom MUC1-ST og Gal3, og de intracellulære mekanismene som de kan sette i gang.

Preface

This thesis is submitted to the Department of Biotechnology and Food Science at the Norwegian University of Science and Technology in partial fulfilment of the requirements for the Master of Science in Chemical Engineering and Biotechnology. The work has been carried out from January to June 2017. The experimental part of the thesis was conducted in the Biopolymer laboratories of Section for Biophysics and Medical Technology at the Department of Physics.

I would like to thank my supervisor Associate Professor Marit Sletmoen for great feedback, suggestions, and helpful conversations. I would also like to thank Research Associate Gianfranco Picco, at the King's Collage, London, for proposing this project in collaboration with Associate Professor Marit Sletmoen.

Professor Bjørn Stokke has been invaluable as he provided the data analysis programs and tweaked them as necessary during this work. I also wish to thank Senior Engineer Gjertrud Maurstad for always being available to help, answer questions regarding the experiments, and especially in assisting the experiments conducted on the AFM equipment for imaging.

In addition, I would like to thank Master Student Øystein Haug and Master Student Katja Siarpilina for helpful conversations, discussion, and insights.

Contents

List of Figures

List of Tables

Abbreviations

AFM	Atomic force microscopy
Akt	Protein Kinase B
Asp	Asparagine
BSA	Bovine serum albumin
CD	C-terminal domain
CRD	Carbohydrate recognition domain
DFS	Dynamic force spectroscopy
EGFR	Epidermal growth factor receptor
FGFR3	Fibroblast growth factor receptor 3
Gal3	Galectin 3
GalNAc	N-acetyl galactosamine
GlcNAc	N-acetylglucosamine
LacNAc	N-acetyllactosamine
MAPK	Mitogen-activated protein kinase
MET	Heptocyte growth factor receptor
MGL	the macrophage galactose-type C-type lectin
MUC1	Human mucin 1
ND	N-terminal domain
Neu5Ac	N-acetylneuraminic acid
OT	Optical Tweezer
PI3K	Phosphatidylinositol-3 kinase
PDGFRβ	Platelet-derived growth factor-β
PTS	Domain on MUC1 rich in proline, threonine and serine
ST	NeuNAcα2-3Galβ1-3GalNAcα1
T	Galβ-3GalNAcα1-
Tn	GalNAcα1-
Wnt	Family of growth factors

Symbols

Symbol	Unit	Explanation
d	m	Displacement
F	pN	Force
f_β	N	Force
$f*$	N	Most probable rupture force
G	J/mol	Gibbs free energy
k	N/m	Spring constant
k_B	J/K	Boltzmann's constant
k_{off}	s^1	Dissociation rate
k_{on}	s^{-1}	Association rate
N	-	Number of measurments
k	N/m	Spring constant
R_a	-	Image roughness average parameter
r_f	N/s	Loading rate
T	K	Temperature
x	m	Displacement
x_β	m	Projection of energy barrier
z_j	m	Height
α	-	Polarisability
β	-	Detector sensitivity
τ_0	-	Bond liftime

Chapter 1

Introduction and theory

Galectins are a family of widely distributed sugar-binding proteins characterized by a specificity for β-galactosides. These lectins are assumed to be involved in diverse biological phenomena critical for multicellular organisms. The highly glycosylated mucins are secreted proteins that protect epithelial cells, but also include more complex transmembrane proteins, such as the human mucin 1 (MUC1), involved in cell repair and survival. MUC1 is an oncoprotein aberrantly expressed at high levels in most human carcinomas. Elevated levels of MUC1 and Galectin 3 (Gal3) are associated with poor prognosis in a variety of malignant tumors. Their cooperative function include cell adhesion and activation of internal signalling pathways. An improved understanding of their physiological role and interaction requires an improved understanding of the Gal3s glycanbinding specifcity. Gal3 is known to bind the MUC1-T, but we have preliminary data indicating that it might bind MUC1-ST as well. The aim of this project is thus to further investigate the substrate specificity of Gal3 lectins, using atomic force microscopy (AFM).

The aim of this project is to investigate and compare the abilities of Gal3 to bind MUC1-T, MUC1-ST, MUC1-Tn, and MUC1-Naked.

1.1 Mucin1

1.1.1 Structure

Mucins are a family of proteins containing a tandem repeat structure with a high proportion of proline, threonine, and serine (PTS domain). The PTS domain are highly glycosylated. The human mucin family is further divided into secreted and transmembrane proteins. The human mucin 1 (MUC1) is a heterodimiric protein, encoded as a single transcript, and autocleaved into two subunits; the transmembrane subunit, MUC1 C-terminal domain (MUC1-CD), and a mucin component, MUC1 N-terminal domain (MUC1-ND), together forming a noncovalent biomolecular complex[1]. MUC1-ND may extend over 100 nm from the cell[2], and act as a physical barrier, protecting the cells from foreign object and stress from the external environment, such as toxins and microorganisms[3].

1.1.2 Function

In short, the MUC1-ND is highly glycosylated and contributes to the mucous gel, important for protection of the cells, and the MUC1-CD functions as receptor for cell signalling[4], and is also important in association with cell protection by influencing cell growth, survival and inflammation[1].

MUC1 expression is up-regulated in response to infection by bacteria, which can lead to chronic inflammation, and prolonged activation and expression of MUC1, which in turn may lead to exploitation of its growth- and survival-promoting effects, and development of cancer[2]. MUC1 has been shown to be an important factor for cell growth, but also influences metastases (spreading of cancer) and regulation of gene expression, and is crucial for maintaining the stemness (the ability to renew and differentiate) in stem cells and embryotic cells[5]. Mucins are overexpressed in cancer cells, and in the US, about 64% of diagnosed tumors are estimated to have high levels of MUC1 expression[3]. During oncogenesis, MUC1-ND is shed from the cell, and circulating MUC1 and MUC16, another family of mucins, are therefore used to monitor the clinical course of patients with breast and ovarian cancer respectively[2]. MUC1 is therefor considered a highly attractive target for anticancer treatment[2, 6].

Epithelial cells, the cells lining organs and surfaces facing the lumen and external environment, such as the intestines, exhibit a polarized structure. The apical side, facing the exterior/environment, is often crucial as a protective barrier, whereas the basolateral membrane, facing surrounding cells, participate in cell-cell interaction[2]. The polarized structure of these cells is illustrated in Figure 1.1.1.

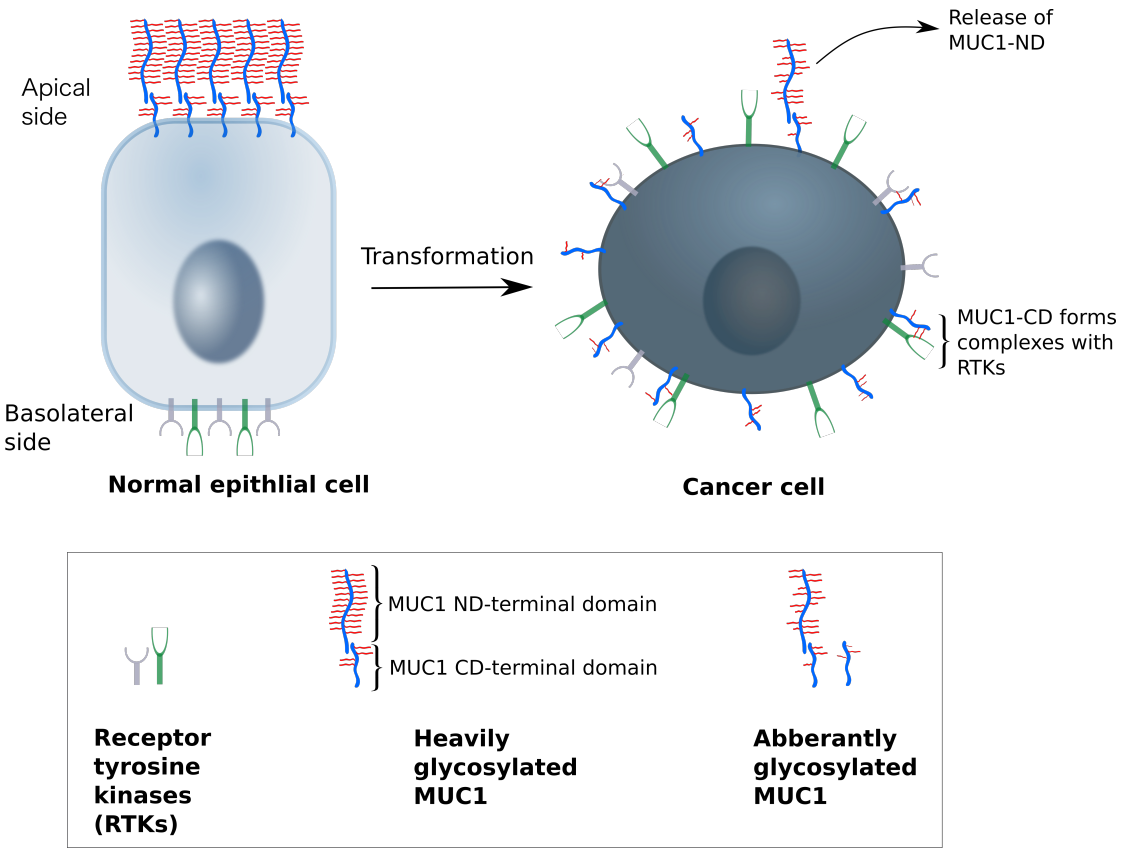

Figure 1.1.1: MUC1 expression and polarity in normal cell versus MUC1 overexpression and loss of polarity in cancer cells (cells undergone transformation). In normal cells, MUC1 is localized at the apical side, and growth factor receptors at basolateral side. Cancer cells have lost their polarity, allowing MUC1 to interact with growth factor receptors. After transformation, the MUC1-ND is shed from the cell. The figure is adapted from from Nath, 2014, and Kufe, 2013 -[5, 4].

The transmembrane mucins are normally localised at the apical membrane. However, when an epithelial cell undergoes transformation (the process cells undergoes when adapting cancer traits) and becomes depolarized, mucins are relocated and expressed all over the cell, facing both the environment and adjacent cells, as illustrated in Figure 1.1.1. After the MUC1-ND subunit are shed from the cell surface, MUC1-C van function more freely as a receptor[3]. Hence, for depolarized cells, the mucins can interact with basolateral transmembrane proteins, such as the receptor tyrosine kinases[2]. The overexpression of mucins contributes to oncogenesis by promoting receptor tyrosine kinase signalling, loss of epithelial cell polarity, activation of growth and survival pathways and down-regulation of stress-induced death pathways[2].

MUC1 overexpression and release of MUC1-ND from the membrane to the cytoplasm and relocalization the the nucleus allows for MUC1-CD to interact with a range of transcription factors, and blocking promotor of target genes[6]. MUC1 contributes to the activation of the human epidermal gorwthfactor receptor 2 (ERBB2), responsible for loss of tight junction function, and thus polarity of epithelial cells[2]. MUC1 is also involved in adherens junctions; in cancer cells, when MUC1 is overexpressed, MUC1-CD can bind β-catenin, and prohibits the interaction between β-catenin with α-catenin and E-cadherin, usually forming the adherens junctions and cell-cell adhesions[2]. The interaction between MUC1 and β-catenin promotes activation of the Wnt pathway, linked to cell growth and oncogenesis (formation of cancer)[2, 7, 8]. MUC1 can also associate with other receptor tyrosine kinases (RTKs) such as fibroblast growth factor receptor 3 (FGFR3), platelet-derived growth factor-β(PDGFRβ), anHepatocyte growth factor receptor (MET), and contributes to the their downstream signalling pathways[3, 1].

1.1.3 Glycosylation

Most proteins and lipids have glycans covalently attached to them, and these glycans constitute most of the variations in biological systems[9]. Not only is MUC1 overexpressed in carcinomas, but the glycosylation patterns are also altered[10], as illustrated in Figure 1.1.1. Such alterations in glycoproteins are common during carcinogenesis[11].

In O-glycosylation of mucins, N-acetylgalactosamin (GalNAc) is covalently linked to a serine or threonine residue on the protein[8]. This glycan structure is called the Tn antigen. The GalNAc can be further elongated by other glycans, such as galactose, sialic acid, fucose, and N-acetylglucosamine[12]. If the GalNAc is further extended by galactose, a T antigen is formed[12]. Normally, further extension is made by addition of N-acetylglucosamine (GlcNAc) to the GalNac, forming a branched structure that can be further elongated[13]. However, in breast carcinomas, one often find truncated glycans with average sizes of 3-4 monosaccharide units[14], such as Tn, T, and ST, as illustrated in Figure 1.1.2. The ST antigen is a further elongation of T with N-Acetylneuraminic acid (Neu5Ac)[13]. The relative amount of these glycans in different breast carcinomas cell lines has been determined. Reported values for MUC1-T varies from trace amounts to 12.9%, and for MUC1-ST between 2.3 and 45.9%[14] and are presented in Table 1.1.1, along with the structure of the ST, T, and Tn glycans.

Table presents the name and structure, as well as reported relative amounts, of the three different glycan structure mentioned found on MUC1.

Table 1.1.1: The glycan composition of the MUC1 proteins used in this thesis, and the relative amount of MUC1 with these glycans in verious breast carcinomas cell lines[14].

Name	Glycan structure	Relative amounts expressed
MUC1-Tn	GalNAcα1-	-
MUC1-T	Galβ-3GalNAcα1-	up to 12.9%
MUC1-ST	NeuNAcα2-3Galβ1-3GalNAcα1-	up to 45.9%

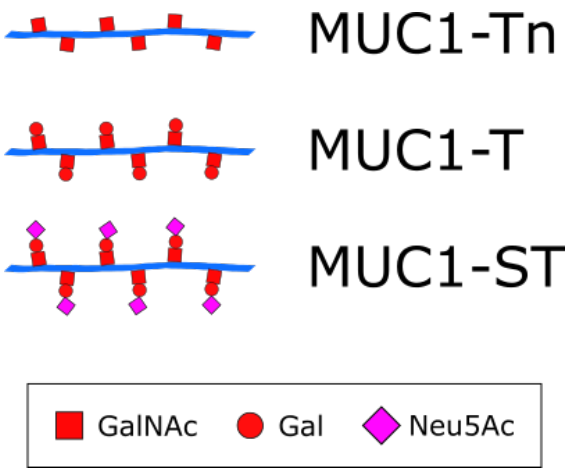

Figure 1.1.2: Schematic representation of truncated O-linked glycosylation of MUC1 associated with cancer. MUC1-Tn consist of a GalNAc residue, MUC1-T is a disaccharide formed by extension of MUC1-Tn with Gal, and MUC1-ST is an extension of MUC1-T with Neu5Ac.

1.2 Galectin 3

1.2.1 Structure

The lectin Galectin 3 (Gal3), a 29-35 kD protein, has a carbohydrate recognition domain (CRD) consisting of 130 amino acids forming a globular structure, which serves as a binding site for β-galactosides[15]. Unlike other galectins, Gal3 also possesses a N-terminal domain (ND), rich in proline and glycine[15]. The ND is essential for biological activity, amongst its many functions is the participation together with the CRD in oligosaccharide binding, and the mediation of the formation of multivalent pentamer structures in the presence of multivalent ligands[15].

1.2.2 Function

Lectins are carbohydrate binding proteins with high specificity and affinity[16]. Gal3 is found in diverse types of cells and tissues, both intracellularly and extracellularly[15], where it engages in specific interactions with a variety of proteins. Gal3 is involved in cell growth, cell adhesion, cell-cell interaction, immune reactions, mutagenesis and metastasis[15, 17, 18]. Gal3 is a β-galactoside-binding lectin, binding poly-N-acetyllactosamine (LacNAc) structures[11], including MUC1-T. Research has revealed that this protein is associated with anti-apoptotic characteristics of breast-carcinoma cells[19, 20] and plays a crucial role in regulation of cell adhesion[21]. More precisely, it influences the probability for detachment of cells from primary tumor and adhesion of circulating cancer cells on to the walls of blood vessels[18].

1.3 Importance of Galectin3-MUC1 interactions for cancer progression

Cancer is characterized by rapid and uncontrolled cell proliferation, as well as increased ability of cancer cells to spread and survive in new environment and tissue, leading to metastasis. These features develop over time, as oncogenes are up-regulated, and tumor suppressor genes are down-regulated[22]. Overexpression of MUC1 in cancer cells has been shown to induce expression of Gal3, suggesting a coordinate expression of the two proteins[23], both with oncogenic functions, as described in section 1.1.2 and1.2.2. In addition, Gal3 can acts as a cross-linker between MUC1 and transmembrane kinases, such as the epidermal growth factor receptor (EGFR)[15, 23], activating oncogenic pathways. It has also been suggested that Gal3 is responsible for

phosphorylation of MUC1, and thus activation of mitogen-activated protein kinases (MAPKs) and Phosphatidylinositol-3 kinase/Protein Kinase B (PI3K/Akt) signalling pathways without co-interaction with EGFR, although co-interaction between MUC1 and other tyrosine kinases mediated by Gal3 could be possible[24]. Several recent studies has concluded that PI3K/Akt is an important determinant of cell survival (triggered by growth factors, extracellular matrix and other stimuli)[22].

1.3.1 Gal3 based bridge formation between MUC1 and EGFR results in receptor activation

Glycosylation of MUC1-CD at Asp-36 functions as a binding site for Gal3, and allows Gal3 to create a bridge between MUC1-CD and EGFR[23, 4], one of the tyrosine receptor kinases. Interaction between Gal3, MUC1-C and EGFR promotes endocytosis and recycling of EGFR to the nucleus. The interaction also promotes EGFR-dependent activation of the PI3K/AKT pathway, involved in cell proliferation, apoptosis and cell migration[4, 25], as depicted in Figure 1.3.1. This signalling triggered by Gal3 binding to MUC1, was reduced when monovalent Gal3 was used, suggesting that the multivalent conformation of Gal3 is important for this interaction[24]. In this particular study, an EGFR inhibitor was introduced, but no reduction in signalling was detected, suggesting that the Gal3-MUC1 interaction is key. This hypothesis was further strengthened by the observation that Gal3 and MUC1 was similarly distributed on the surface of cancer cells[24].

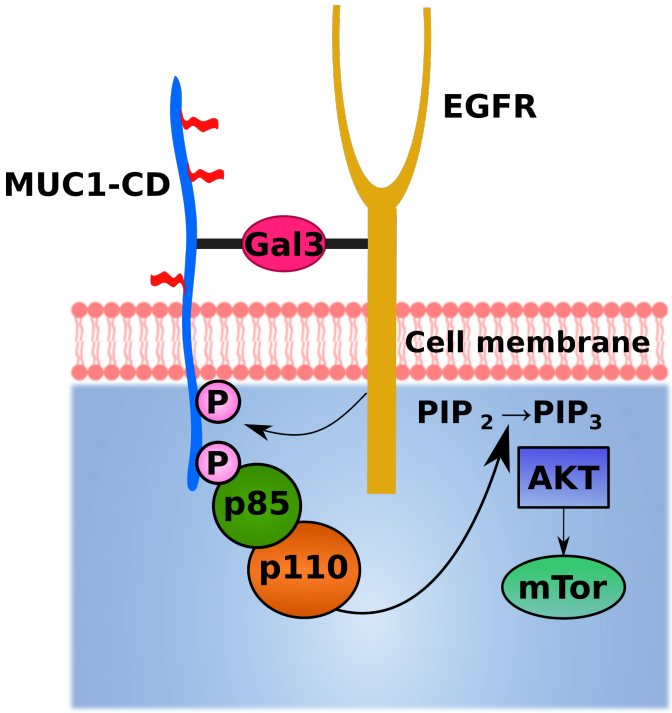

Figure 1.3.1: Interaction between MUC1-CD and EGFR at the cell membrane facilitated by Gal3 activates the PI3K/AKT pathway. MUC1-CD is phosphorylated by EGFR. The activated MUC1-CD will in turn activate the PI3K-AKT pathway. The figure is adapted from Kufe, 2013[4].

1.3.2 Gal3-MUC1 interactions promotes cancer cell adhesion to endothelium

Cell adhesion is a common trait in tumor progression and metastasis, which involves the migration of tumor cells within the primary sites, invasion to blood or lymphatic vessels, and adherence to endothelial cells at secondary sites[18]. It has been demonstrated that circulating Gal3 increases adhesion of MUC1-expressing cancer cells to blood vessel endothelial cells[26, 27, 28]. Proposed mechanisms for this includes a redistribution and clustering of MUC1 on the cancer cell surface as its interaction with circulating Gal3, exposing the smaller cell adhesion molecules, and allowing them to interact with surrounding endothelial cells. Thus, the interaction between circulating Gal3 and cancer cells with appropriately glycosylated MUC1 promotes metastasis.

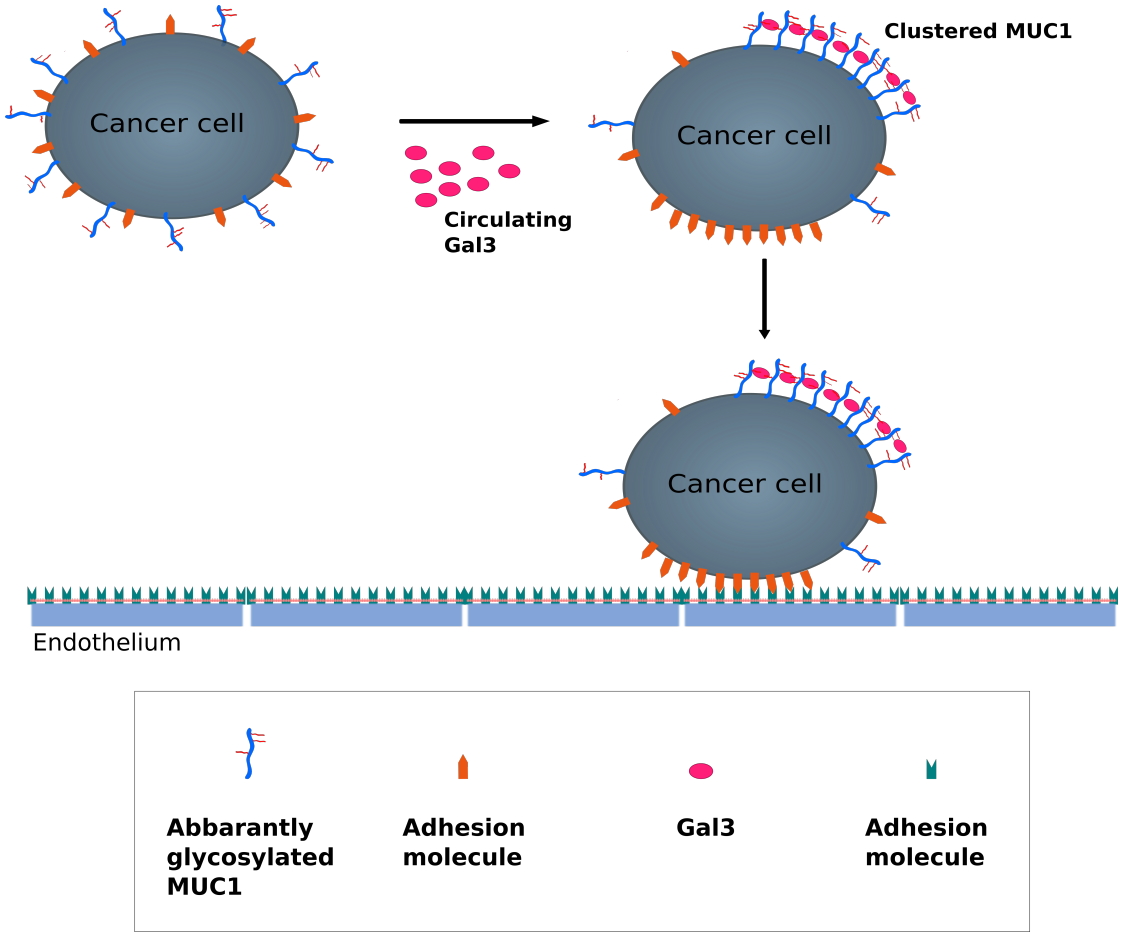

Figure 1.3.2: Proposed mechanism for adhesion of cancer cells to endothelium by interaction between MUC1 and Gal3. The interaction between circulating Gal3 and MUC1 on the cancer cell surface leads to a redistribution of MUC1 and the exposure of smaller cell adhesion molecules. The figure is adapted from Yu, 2007[26].

Furthermore, the clustering of MUC1 induced by the interaction with circulating Gal3 also promotes aggregation of the cancer cells circulating in the bloodstream. Aggregated cancer cells have an increased likelihood of surviving in the blood stream compared to single cancer cells, thus this interaction also enhances the proliferation of cancer cells[28].

1.3.3 Gal3-MUC1 interactions promotes activation of signalling pathways

In addition to promoting aggregation of cancer cells and adhesion of cancer cells to endothelial cells [26, 27, 28], interaction of Gal3 with MUC1 also result in downstream signalling. More precisely, this interaction is reported to activate MAPK and PI3K/AKT signalling pathways, known to enhance cell proliferation and motility[24, 29, 30].

1.3.4 Interaction between Gal3 and MUC1 are determined by the glycosylation of MUC1

As mentioned in section 1.3.1, 1.3.2 and 1.3.3, the interaction between Gal3 and MUC1 is important for cancer progression, and for that reason, the understanding of this mechanism is of vital importance to provide new insight into cancer treatment. It is known that Gal3 binds MUC1-T, but if Gal3 also holds the ability to bind MUC1-ST, this is important new information, as MUC1-ST is just as commonly expressed on breast carcinoma cells as MUC1-T, see Table 1.1.1 on page 7.

1.4 Atomic Force Microscopy

In atomic force microscopy (AFM), which first appeared in 1986[31], forces acting between atoms or molecules are quantified. The instrument is set up with a cantilever with an AFM tip, and any change in the tips position are measured by a laser that is reflected off the cantilever on to which the tip is mounted and detected by a split photodiode. The changes in the tips position is caused by forces acting between the tip and a sample surface. Although this thesis focuses on AFM measurements used to investigate inter-molecular interactions, AFM was also used to describe the topography of the surfaces used for the interaction measurements.

1.4.1 AFM used as an imaging tool with nanoscale resolution

The basic idea behind AFM was to let a sharp tip scan a surface while detecting interaction between the tip and the surface[32]. The AFM system can detect changes in the tips position while scanning over a surface, and map a three-dimensional surface topography image based on height measurements. The height measurements are displayed as colors with a gradient, usually dark colors representing the lowest valleys of

the surface, and light colors representing the highest peaks of the surface[33]. The advantages of using such a technique compared to other microscopy techniques are the enhanced resolution; while optical microscopy can generate images with resolution up to 250 nm, AFM can generate images with sub-nanometer resolution[32, 34]. This technology provides the ability to map distributions of single molecules on a surface[32].In AFM, the resolution concept is divided into lateral and vertical resolution. The vertical resolution is limited by thermal noise generated by vibration of the cantilever, hence the minimum detectable height depends on the spring constant. Lateral resolution is typically smaller than the vertical resolution, as this depends on several factors, one of them being the geometry of the cantilever. If the tip has a pyramid-like shape, the lateral resolution will go down, as sharp peaks on the surface investigated will appear as wider than they are in reality[35].

Typically, AFM provides two imaging modes; contact mode and dynamic mode[32]. In contact mode, the sharp tip is in constant contact with the sample, likely to distort or damage the surface while scanning, especially if a fragile sample is under investigation[34]. The dynamic mode is further divided into two sub-categories; non-contact mode and tapping (intermittent) mode[34]. In the non-contact mode, the cantilever and tip is vibrated near its resonance frequency, and the motion of the tip, affected by van der Waals forces and other long-range forces between the surface and the tip, are detected. In tapping mode, the vibrating tip is in contact with the surface while scanning, but only for a short period of time. Although the tip is in contact with the sample in tapping mode, the stress on the sample applied by the tip is greatly reduced compared to contact mode[32].

The three-dimensional topography image provides the opportunity to measure peak-to-valley distances, and other statistical parameters based on the height measurements. One of the most common parameter to use when comparing surfaces is the image roughness average parameter, R_a, which is an average value based on height in accordance with the following equation:

$$R_a = \frac{1}{N} \sum_{j=1}^{N} |z_j| \tag{1.4.1}$$

where N is number of measurements, and z_j is the height, thus R_a is the arithmetic average of the absolute values of the surface height deviation measured from a mean plane[36]. This commonly used parameter has several advantages, the foremost being that it is very easy to obtain. However, one should not forget that this parameter reflects the average property of a surface. Two surfaces with very different height profiles could thus have the same R_a value.

1.4.2 AFM as a tool for measuring inter-molecular interactions

When atomic force microscopy is used for investigation of inter-molecular forces, a cantilever with attached molecules are moved towards a surface studded with another type of molecule[37]. As the molecules come in contact, and further force is applied, the cantilever is deflected away from the surface. Usually, a flat surface on the atomic scale are used, such as freashly cleaved mica, or glass. After bringing the molecules in contact, the distance between the AFM tip and the surface is increased and the molecules attached to these surfaces are thus moved apart, as illustrated in Figure 1.4.1. It is possible to measure the forces acting between the molecules, by utilzing Hook's law: $F = kd$, where F represents the rupture force, k represents the spring constant and d represents the cantilever deflection[31].

Several variants of AFM are possible, depending on the samples immobilized: in chemical force microscopy, chemical groups are immobilzed, in single-molecule force spectroscopy biobolecules are immobilized, and in singel-cell force spectroscopy cellular structures are immobilized. Single-molecule force spectroscopy are commonly used for the investigation of antigen-antibody interactions[31]. When such biomolecules are investigated, the immobilization process must ensure that the native structure and function of the molecules are preserved, that binding sites are available, that the molecules are immobilzed in a uniform matter on to the surfaces, that the attached molecules not detaches during measurements, and that minimal non-specific interaction take place. For these reasons, molecules are normally covalently attached to the surfaces, making sure that observed bond ruptures are of the biomolecular complex, and not detachment of immobilized molecules. To make sure that no interactions between the functionalized cantilever and the surface sample occur, and that the molecules can move freely so that the binding sites are available, linkers are commonly used between the surfaces and the investigated molecules. The linker is normally a linear oligomer or polymer, and the increased distance between the immobilized molecules and the surface decreases the possibility of the mentioned interactions between the surfaces. In addition the linker allows the proteins rotational freedom, thus increasing the likelihood of specific interaction to occur.[31]

When studying molecular interaction using AFM, a frequency of one binding event in every 5-10 touches is considered optimal.The reason for this is that at this optimal frequency, the probability for formation of interactions between a single pair of molecules, as opposed to multiple molecular pairs, is optimized[37]. The density of the molecules on the AFM tip should be tweaked during experimental studies, to reach a probability for observing signatures in the force-versus-distance curve reflecting interaction events in this range. After obtaining a high number of force versus z-piezo retraction curves, the rupture force is determined for each of the molecular bond rupture

events, as well as the associated loading rate. This information is further processed and divided into subsets of loading rates, each presented as a histogram of rupture forces. The peak in each the histogram distribution will reflect the most likely bond rupture force[37].

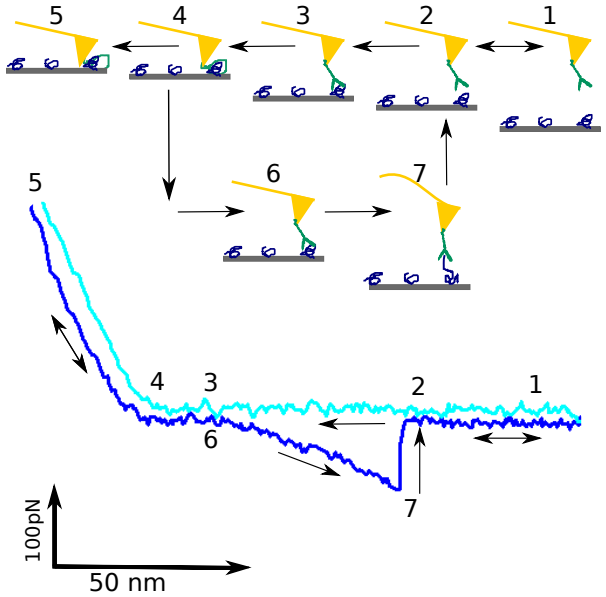

Figure 1.4.1: Inter-molecular interaction event detected by AFM. A molecule attached to the AFM tip interacts with a molecule present on the surface (points 1-5). At point 5 the cantilever is deflected away from the surface. During retraction (point 5-7, 2, 1) the force increases until rupture occurs (7-2). The figure is adapted from Hinterdorfer, 2008[38].

If an interaction between the molecules has occurred, the cantilever will be deflected towards the surface, until enough force is applied over time to rupture the interaction. Note that the forces studied here are specific, non-covalent interactions. Deflection of the cantilever is detected by a laser pointing at the tip, and reflected on to a position sensor, as illustrated in Figure 1.4.2. Whilst the cantilever is deflected, the position of the laser on the detector is also changed. If using a position sensitive detector, more precisely a split photo diode consisting of four sections (Figure 1.4.2), the changed location of the laser on the surface of the detector will lead to a relative change of strength of the volt signal produced in each of the detector quadrants. During calibration, schematically illustrated in Figure 1.4.3, the two conversion factors sensitivity, β, and the spring constant k, is determined. Sensitivity is a conversion factor that gives the relationship between the change in the location of the laser spot on the photodiode surface and the amount of deflection of the cantilever. The spring constant is a conversion factor that gives the relationship between amount of deflection of the cantilever and the force applied on to the cantilever.

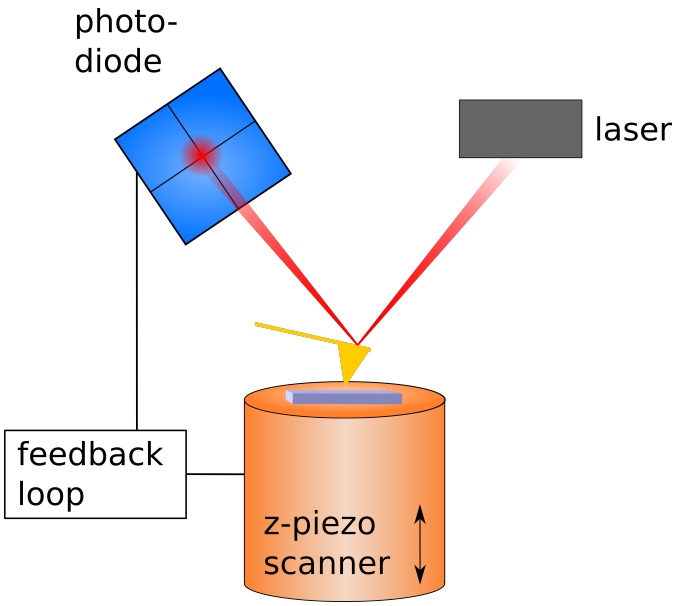

Figure 1.4.2: The setup of the instrument. The spring is deflecting away from the surface after the cantilever has approached the surface. A laser pointing at the tip of the cantilever, and reflected on to a sensor, detecting any deflection.

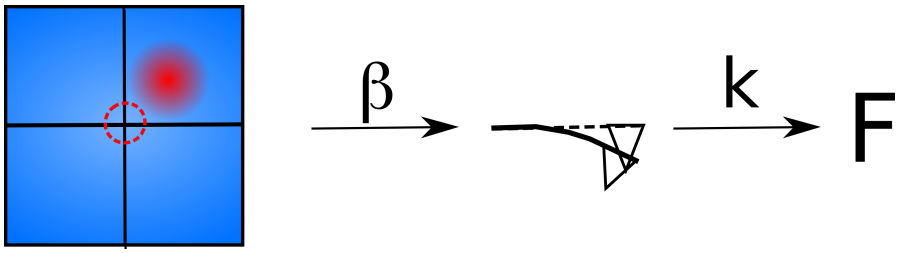

Figure 1.4.3: Schematically illustration of the calibration of AFM, where β and k are conversion factors. More precisely, β is the sensitivity, and k is the spring constant.

Application of AFM to quantify ligand-receptor interactions

Specific, non-covalent interactions between a receptor and a ligand can create a stable biomolecular complex. These interactions consist of electrostatic interactions, hydrogen binding, $\pi - \pi$ interactions, van der Waals forces, and hydrophobic interactions, and the total strength of the interaction can compete with the covalent ones[39].

If a ligand-receptor interaction, such as MUC1-Gal3, is investigated with AFM, a typical saw-tooth structure can be observed, as illustrated in Figure 1.4.4. For MUC1-Gal3, the saw-tooth structure is characterized by multiple peaks, or rupture events, due to the tandem structure of MUC1 with several possible binding sites for Gal3[40, 41, 42]. These multiple peaks can be observed due to MUC1 being attached to several Gal3 molecules, or that more than one MUC1 is attached to Gal3, as illustrated in Figure 1.4.4 A and B respectively. Such multiple peaks can complicate the extraction of parameters characterizing the energy landscape of the biomoleular complex formed, thus a number of measurements should be performed to alleviate this disadvantage. In addition, the already complex stochiometry of these reactions make the definition of the thermodynamic and kinetic parameters difficult. This is discussed in greater detail in section 1.6 [31].

It may be impossible to acehive force-versus-distance curves with only one peak when investigating reeptor-ligand interactions. If multiple peaks are present also after optimizing the molecule density on the cantilever and surface, it could mean that multiple interactions do occur within the same ligand-receptor complex. This may be the case for Gal3-MUC1 interactions, due to the likely pentamer conformation of Ga3, and multiple glycans per MUC1.

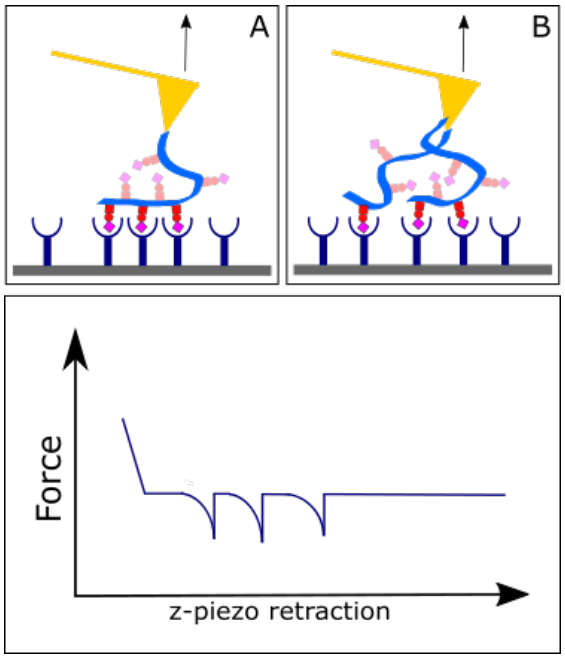

Figure 1.4.4: Schematic illustration of the typical saw-tooth structure in the force-versus-distance curves observed due to the tandem structure of MUC1. The separated peaks can arise due to MUC1 interacting with several Gal3 (A), or multiple MUC1 interacting with Gal3 (B).

1.4.3 Non-specific interactions

Rupture events concentrated around the contact point between the AFM tip and the surface might be caused by non-specific interaction between the AFM cantilever and the surface and are usually not included for further analysis which aim is to investigate molecule interactions[43, 44]. Such non-specific interactions are thought to be caused by interaction between the surface and the AFM cantilever, allowing the protein on the cantilever to unfold[45]. This may be reduced by covering the mica slide by a substrate, such as agarose beads, that absorb some of the force when the cantilever come in contact, but also reduce electrostatic interaction between the cantilever and the hard surface, as suggested by Celik *et. al.*[45]. As mentioned in section 1.4.2, a linker can be utilized to reduce the occurrence of non-specific interactions, especially when dealing with small, globular proteins, and can increase likelihood of specific interactions as the proteins are given more rotational feedom.

Non-specific interactions is reported to account for 15% to 85% of force curves depending on the complex studied and the type of immobilization used [31]. To confirm specific interactions, the biomolecular complex is investigated with an inhibitor present. These measurements are reported to also show some variance in interaction frequency, although this is drastically decreased compared to investigation without inhibitor. Thus, obtaining sufficient amount of data is crucial to obtain a dataset satisfying statistically significant distrubutions[31]. It is also possible to investigate specificity by removing or replacing one of the immobilized molecules, but the changes in the properties of the surfaces may lead to an increase in non-specific binding events.

1.5 Optical Tweezers

In optical tweezers (OT), a focused laser beam is used to trap a small dielectric bead to which molecules of interest are attached[42]. The bead experiences radiation pressure, and a strong, electromagnetic field gradient near the focus of the laser beam polarises the trapped bead, which in turn will experience a force proportional to the light intensity[42];

$$F = \alpha \nabla I_0 \tag{1.5.1}$$

where F is the force, I_0 is the light intensity, and α is the beads polarizability. The wavelength used is often near the infrared part of the spectrum to avoid damage to the attached molecules[42]. The OT measures the three-dimensional displacement of the trapped bead[41], after calibration of the trap stiffness has been performed. The trap

stiffness can be calibrated amongst other ways through variance, as depicted in Figure 1.5.1. The trap typically has a lower stiffness than those associated with the AFM, typically ranging between 0.01 and 1 pN/nm[42]. This is a factor of hundred lower as compared to AFM. Due to these properties of the OT, forces can be quantified.

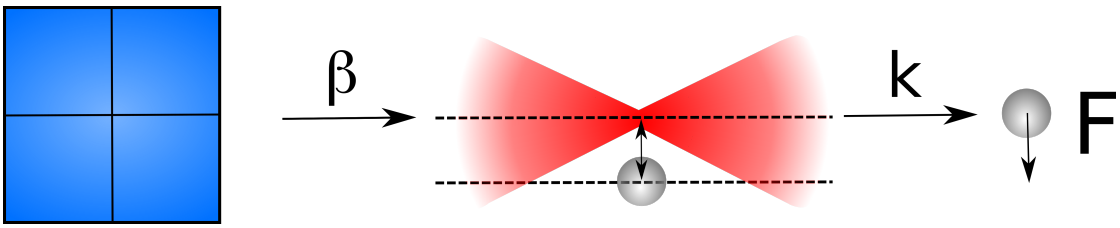

Figure 1.5.1: Schematic illustration of the conversion factors and parameters used to determine forces acting on a bead when using OT. Changes in diffraction patterns detected by the diode are converted into a displacement coordinate, x, by multiplying with sensitivity, β. The displacement, x, is translated into a force by multiplying with trap stiffness, or spring constant, k.

When investigating interaction between two different molecules, a dual-trap mode can be used. In a dual-trap setup, the laser beam is split into two separate beams, each creating an optical trap. One molecule is attached to a bead of a specific diameter, the other molecule is attached to beads with different diameter, enabling to distinguish them. The two optical traps are used to trap two beads characterized by different diameter, and thus displaying different surface molecules, and forces acting between them are continuously recorded while one of the beads are moved into contact with, and away, from the other.

1.6 Dynamic force spectroscopy

Inter-molecular bonds between biomacromolecules arise mainly from non-covalent interactions (van der Waals forces, $\pi - \pi$ interactions, electrostatic interactions, hydrogen bonds, and hydrophobic interactions), and have limited lifetime, hence they will eventually rupture if a force is pulling on them for a sufficient time[46, 47, 48]. When utilizing ultrasensitive force probes, such as AFM, the bond strengths of these interactions are quantified by pulling on the molecules interacting, each attached to a separate surface[46, 47]. Dynamic force spectroscopy is an experimental approach that enables the study of the binding forces between individual molecules[47]. Different force probes can be utilized to realize the studies, including AFM and optical or magnetic tweezers. In AFM based dynamic force spectroscopy, the inter-molecular

bonds are exposed to an external force that increases with time, defined as the loading rate $r_f = \Delta f / \Delta t$. A plot of the bond strengths against the logarithm of the loading rate, provides the basis for dynamic force spectroscopy and contains information about the specific energy landscape[46]. Because of the stochastic nature of non-covalent interaction, a large number of observation must be obtained to alleviate this disadvantage and produce a robust estimate for the parameters characterizing the energy landscape[44, 46].

Biological complexes with non-covalent interactions can have energy landscapes comprised by various intermediate states associated by low lifetimes. During unfolding of a protein, such as a DNA strand, different forces can act between different parts of the protein as they come in close proximity and form temporarily intermediates until fully unfolded. Hence, during dissociation of biological complexes, the complex must overcome several activation barriers, characterizing the energy landscape. For simplicity reasons, this complex energy landscape consisting of different activation barriers is projected on to a curvilinear coordiate system, called the reaction coordination, x.

During unfolding or dissociation, the system must overcome one or several activation barrier. In other words; the system must obtain a free energy higher than those of the reactants/products or the two states. The energy landscape is defined as the free energy landscape containing free energy of all bound and unbound states and the characteristic energy barriers, or free energy peaks for the transition states between them, along the reaction coordinate, x. When two molecules with mutual affinity for each other, A and B, interact with each other in solution, the complex, AB, exists in a time dependent matter after the equation[48]:

$$\frac{d[AB]}{dt} = k_{on}[A][B] - k_{off}[AB] \tag{1.6.1}$$

Here [A], [B], and [AB] is the concentration of the two molecules and the complex between them, k_{on} is the association rate and k_{off} is the dissociation rate[24].

In a mechanical experiment, such as AFM experiments, an external force is applied to a molecular interaction over a certain period of time[47]. Application of forces to a biomolecular complex alters the free energy landscape, and the activation energy is lowered[31]. Bell proposed a model for this bond-breaking in presence of external force based on tranisiton state theory[31, 48]. He first predicted that the effect of application of an external force on a biomolecular complex would be a decrease in free activation energy by a factor proportional to applied force[48]. Usually in AFM studies, the two molecules anchoring the bond is moved apart as one of the surfaces is pulled away at a constant rate $\Delta x / \Delta t$, so that the force applied increases over time[47]. Hence, the

loading rate $r_f = \Delta x/\Delta t = k_f(\Delta x/\Delta t)$ is defined by the retraction speed and the spring constant, k_f, of the spring which the molecule is attached to[47].

The above gave rise to the well recognised Bell-Evans model, where it is assumed that the k_{on} is minimal, compared to k_{off}, as external force along the reaction coordinate is applied, making the k_{on} expression negligible. According to the Arrhenius equation, the disassociation rate will then increase with the activation energy in accordance with the following equation:

$$k_{off} \propto e^{\frac{-\Delta G^*}{k_B T}} \tag{1.6.2}$$

Here ΔG^* is the activation energy, k_B is Boltzmann's constant, and T is the absolute temperature[24].

According to the Bell Evans-model, as an external force is used to pull on a bond, the following equation should be applied to calculate the new dissociation constant[24][48], taking into account the applied force aiding the thermal activation:

$$k_{off}(F) = k_{off}(0)e^{\frac{f x_\beta}{k_B T}} \tag{1.6.3}$$

Where $k_{off}(0)$ is the dissociation coefficient at equilibrium (no external force applied), x_β is the reaction coordinate corresponding to the distance from bound state to activation barrier, f is applied force, k_B is Boltzmann constant and T is the absolute temperature.

Here it is assumed that the applied force is working in the direction of the reaction coordinate until the transition state is reached[47], that the force applied increases linearly with time (constant loading rate), and that only a single couple of molecules are interacting[48]. It is clear here that the disassociation coefficient increases exponentially with force[47]. k_{off} is related to the lifetime of the complex, τ_0 , by the following relationship:

$$\tau_0 = \frac{1}{k_{off}} \tag{1.6.4}$$

As the activation energy is lowered when an external force is applied, the location of the activation barrier with respect to the energy minimum characterizing the bound state in the energy landscape, x_β, is assumed to be constant[47]. The external force induces an increased likelihood of bond dissociation, and the probability of bond survival decreases as depicted in the following equations[48]:

$$\frac{dS(t)}{dt} = -k_{off}(f(t)S(t)) \tag{1.6.5}$$

$$S(t) = e^{\int_0^t k_{off}(t')\,dt'} \tag{1.6.6}$$

One can now obtain an expression for the probability of bond rupture, where $r_f = \Delta x/\Delta t = k_f(\Delta x/\Delta t)$ is used:

$$P(f) = \frac{k_{off}((f))}{r_f} e^{[-\int_0^f \frac{k_{off}(f*)}{r_{f*}} df]} \tag{1.6.7}$$

By using the Bell-Evans assumption and performing the integration, $P(f)$ becomes:

$$P(f) = \frac{k_{off}(f)}{r_f} e^{[\frac{fx_\beta}{k_BT} + \frac{k_{off}k_BT}{x_\beta r_f}(1-e^{\frac{fx_\beta}{k_BT}})]} \tag{1.6.8}$$

The most probable rupture force, f^*, at a specific loading rate, can be obtained by maximizing the equation above:

$$f^* = \frac{k_BT}{x_\beta} ln(\frac{r_f x_\beta}{k_{off}k_BT}) \tag{1.6.9}$$

Hence, the force that most frequently leads to bond rupture at a given loading rate is the peak in the rupture force distribution. The bond strength increases with the loading rate, so there is a linear relationship between most probable force and the logarithm of the loading rate[47]. k_{off}, at zero applied force, and x_β, both characterizing the energy landscape can be obtained from the slope and intercept when the linear relationship between most probable force and the logarithm of the loading rate are fitted to the data[47].

For the determination of most probable rupture force associated with a specific loading rate, the obtained force data must be divided into bins of loading rates, each characterized by a mean loading rate. For the best fit of the Bell-Evans model, the bins should be as narrow as possible, but still consist off sufficient amount of data for a good fit. This is accomplished by making sure the data set is very large.

If there is observed more than one linear region in the plot of most probable rupture force versus the logarithm of the loading rate, this is commonly interpreted as evidence of two or more energy barriers in the energylandscape, characterized by their respective x_β.

Further Development of the Bell-Evans theory by Dudko *et al.*[49, 50] provides a new method for extraction of molecular kinetics, such as interaction lifetime, τ_0. In short; the Bell-Evans model assumes a special case where the energy landscape is characterized by harmonic and sharp energy wells, whereas other geometries of the energy landscape is possible. Dudko *et. al.* included a new parameter representing the geometry of the energy landscapes and proposed a new method for determining τ_0.

Additional development of the theory and its application has emerged during the last years, which includes a new method for selection of force curves and a new way of interpreting and processing force data containing non-linear regions. Friddel *et. al.* [51] developed a method for analysis of force curves after the observation of multiple linear regions in the force versus logarithm of the loading rate spectrums, commonly credited to the discovery of multiple barriers within the energy landscape. These multiple linear regions were taken as evidence that nonlinear regions are common in force measurements, and credited to rebinding events during measurements or the result of multiple bonds. Bizzarri *et. al.* [52] suggest a simpler method for selection of force curves containing signature interaction events, based on the analysis of the noise frequency and recognition of specific frequency associated with biorecognition events. This method has been validated on an antigen-antibody complex and would thus be appropriate to include in this study.

The presented result in this master thesis is based on the traditional Bell-Evans model, although the new developments made by e.g. Dudko *et al.*, Friddel *et. al.*, and Bizzarri *et. al.* could be incorporated to give a higher certainty of the obtained parameters characterizing the energy landscapes. These developments were not implemented, as appropriate resources and sufficient time were not available.

1.7 Atomic Force Microscopy versus Optical Tweezers

Both AFM and OT provides information about molecules and interaction between them, but, amongst other things, typical force range and spring constant differ, as summarised in Table 3.7.1[41, 42]. Combining data from both OT and AFM will provide access to a broader range of forces in the study of single molecule spectroscopy, as seen in previous studies[44].

Table 1.7.1: Comparison of OT and AFM

	Optical tweezer	**AFM**
Typical force range [pN][42]	0.1-100	5-10^5
Typical spring stiffness [pN nm^{-1}][41]	0.05-1	10^5

Chapter 2

Materials and methods

2.1 Materials

- Gal3, R&D Systems, Inc
- N-[3-Trimethoxysilylpropyl]ethylenediamine triacetic acid trisodium salt, 45% in water, abcr GmbH
- N-(3-Dimethylaminopropyl)-N-ethylcarbodiimide hydrochloride (EDC), Sigma-Aldrich
- AFM probe cantilever, model OTR4-10, BRUKER
- Carboxyl-polystyrene beads, 3.07 μm, Spherotech
- Amino-polystyrene beads, 2.07 μm, Spherotech
- HEPES buffer, Sigma-Aldrich
- Calcium dihydro chloride $CaCl_2$,
- Manganese tetrahydro Chloride $MnCl_2$,
- Boric acid, pH5.8

Mucin samples were kindly provided by Gianfranco Picco, King's College, London. All samples used were reported to have high purity. The samples were produced as described in Backstrom *et al.*[53]. The MUC1-ST samples used had Immunoglobulin G (IgG) attached, whereas the MUC1-T, Tn, and -Naked had not.

2.1.1 Equipment

ForceRobot 300, JPK Instruments, Berlin, equipped with high-precision mapping stage.
NanoTracker, JPK Instruments, Berlin, equipt with dual trap mode
MultiMode8, BRUKER, Massachusetts, equipped with PicoForce scanner allowing tapping mode

2.2 Methods

2.2.1 Preparation of samples for AFM investigations

The aim of the procedure is to immobilize Gal3 lectins to mica slides, and MUC1 to AFM tips, as depicted in Figure 2.2.1. The immobilization method was modified from previously reported procedures[54, 55]. Freshly cleaved mica slides and AFM tips were silanized in a 1% solution of N-(trimethoxysilylpropyl) ethylenediamine triacetic in 1 mM acetic acid for 30 minutes, and rinsed in MQ-water. This was done so that proteins could be immobilized on to the mica surface and the AFM tip. AFM tips were then covered in a filtered 100 mM boric acid (pH 5.8) solution containing 0.2 mg/ml mucin (MUC1-ST, -T, –Tn, or -Naked) and about 1.5 mg/ml EDC allowed to incubate on ice for 45 minutes. The EDC facilitates the covalent linkage between the carboxyl groups on the mucin surface and amine groups on the silianized AFM tips. Mica slides were covered in a filtered 100 mM boric acid (pH 5.8) solution containing about 0.01 mg/ml Gal3 and about 1.5 mg/ml EDC allowed to incubate on ice for 45 minutes. The EDC facilitates the covalent linkage between primary carboxyl groups on the Gal3 surface and amine groups on the silianized mica slides. After incubation, mica slides and AFM tips were rinsed and stored in a filtered 100 mM HEPES buffer solution (pH 7.2) containing 1 mM $CaCl_2$ and 1 mM $MnCl_2$. The HEPES buffer was used in oder to create a physiological environment, making sure that the proteins stays in their native conformation. HEPES is a physiological buffer commonly used for cells and proteins. Mn^{2+} and Ca^{2+} was used as metal ions as they are reported to be necessary to keep lectins in their active form[56]. The prepared samples were all used within 3-4 hours, and stored on ice. Both the incubation concentration of MUC1 and Gal3 was selected after trial and error to obtain an ideal protein density on both the AFM tip and the mica surface. All incubation and storage before measurements was done on ice, to avoid denaturation of the proteins.

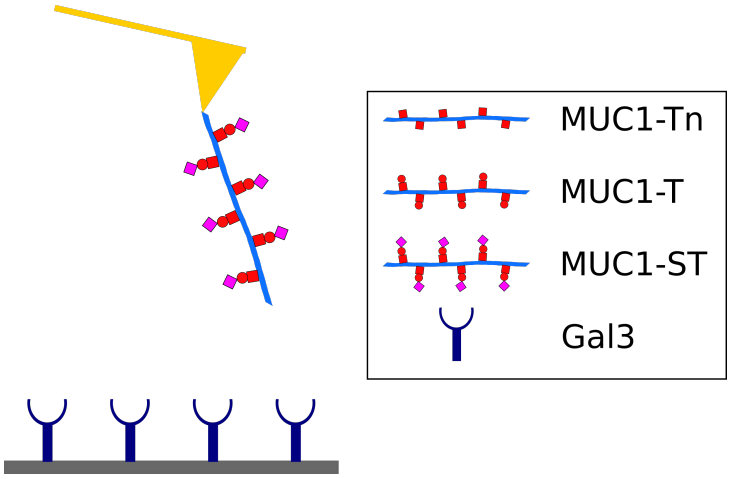

Figure 2.2.1: Schematic illustration of the method used. MUC1, either with Tn glycan, ST glycan, or ST glycan, covalently attached to AFM tip, and Gal3 covalently attached to mica surface.

Preparation of samples for AFM imaging

In order to investigate the outcome of the silanization as well as the successive immobilization of galectins on to the mica surfaces, tapping mode AFM imaging was performed. Two samples of mica slides with Gal3, as well as two samples were just the silanization step was performed, were dried by gently blowing N_2 gas, and than dried in a vacuum pump for 4 hours. The AFM imaging was performed by Senior Engineer Gjertrud Maurstad at Department of Physics.

2.2.2 Preparation of samples for OT investigations

EDC was added to two eppendorf tubes each containing 50 µl of filtered 100 mM boric acid (pH 5.8) to a final concentration of 4 mg/ml. 2 µl of polystyrene beads of diameteres equal to 2 and 3 µm, and fuctionalized with amino- and acid groups, respectively, were added to each of the eppendorf tubes. MUC1-ST was added to the eppendorf tube containing the amino-functionalised polystyrene beads with a diameter of 2 µm to a final concentration of 0.25 mg/ml. Gal3 was added to the eppendorf tube containing the acid-functionalized polystyrene beads with a diameter of 3 µm to a final concentration of 0.01 µg/ml, both allowed to incubate for 45 minutes. The two samples were centrifuged for 1 min at 6000 rpm. Supernatant was removed, and 200 µl HEPES buffer was added. This was repeated one time, then the supernatant was removed, and 200 µl HEPES was added to the MUC1 sample, and 100 µl to the Gal3 sample. 20 µl of each

sample were mixed together. A liquid cell was filled up by approximately two drops of the mix, now ready for analysis with the OT.

2.2.3 Collection of AFM force curves

Interaction between Gal3 and all four types of MUC1 was studied using a ForceRobot300. All measurements were conducted in HEPES buffer (pH7.2) containing 1 mM $CaCL_2$ and 1 mM $MnCl_2$ at room temperature. Experiments were performed with Gal3 immobilized on mica slides, and one type of mucin immobilized to the AFM tip. All measurements were performed using a cantilever with a nominal spring constant of 0.020 N/m.

Additional control experiments were performed, where MUC1-ST and -T was immobilized on to the AFM tip and probed against a silanized mica slide without Gal3. One last control experiment performed consisted of a Gal3 immobilized mica slide and a silanized AFM tip without MUC1.

Interaction between Gal3 and MUC1 was measured on different location on the mica slide studded with Gal3 by setting up an automatic probing series with a 10 by 10 matrix covering a 9 by 9 µm area, and two measurements at each point. The contact time between the cantilever and the surface was set to null, and the z-piezo retraction speed was varied between 2, 1, and 0.5 µm/s. The spring constant for each AFM tip used was determined by measuring thermal fluctuations of the cantilever. The deflection sensitivity for each tip was determined by determining the slope of the line reflecting increase in force per unit length when indenting a functionalized mica surface.

2.2.4 Collection of OT force curves

Interaction between MUC1-ST and Gal3 was also investigated using a NanoScope to confirm the results obtained by the AFM. After optimiziation of the lenses position, beads with different diameters were trapped in the two optical traps. Automated calibration implemented in the software was used. As one bead was held stationary, the other one was moved at a 0.5 µm/s speed so that the two beads would touch, and then moved apart. By detecting any changes in the bead position, a series of force measurements were performed. This was repeated on different sets of beads.

2.2.5 Analysis of force retraction curves

Force retraction curves containing force jumps were interpreted as evidence of an interaction event between Gal3 and the specific mucin immobilized on to the AFM tip, or the polystyrene bread as used in OT. The rupture events from AFM observed in the on to curves obtained in an experimental series were counted and used to determine the fraction of curves containing signature interaction events, P_{int}, for interaction between Gal3 and MUC1-ST, -T, –Tn, and -Naked. The loading rate associated with each force jump both from data obtained with both AFM and OT was determined, using a software developed and kindly provided by Professor Bjørn Stokke (named difordijpkv31d and iNanoTrackerPostProcess2), as explained in Figure 2.2.2. In addition, for the AFM data the position of the force jump relative to the contact point was determined.

For the AFM data, force retraction curves containing force jumps separated from the contact point were gathered for further analysis. If a force retraction curve contained force jumps not separated sufficiently to be able to determine the loading rate, it was rejected.

In the investigation of the energy landscape set by interactions between Gal3 and MUC1-ST and T measured with AFM, the rupture forces were plotted against determined loading rates. The data were grouped into intervals of loading rate, and the mean loading rate, r_f, for each group was determined. The data contained in each group was presented in a histogram and Equation 1.6.8 was fitted to the distribution. In this project a constrained fit of Equation 1.6.8 was performed, keeping x_β constant and equal to the value obtained as explained in the following. Averaged values of x_β were determined by linear regression of the dynamic force spectrum, f^* versus $ln(r_f)$, for each linear region in this representation. The most probable rupture force, f^* , as well as the lifetime of the molecular bond, τ_0, was determined for each interval defined along the axis of increasing force loading rate. Another software program developed and kindly provided by Professor Bjørn Stokke (named ForceSpecAnalysev8) made this data processing and parameter determination possible.

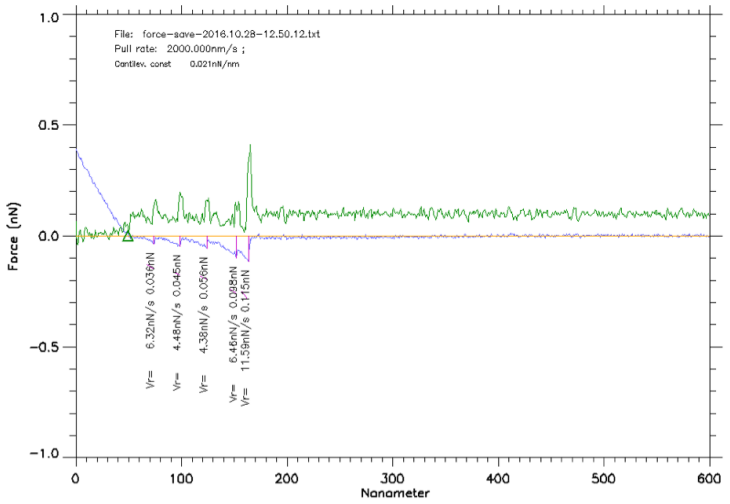

(a)

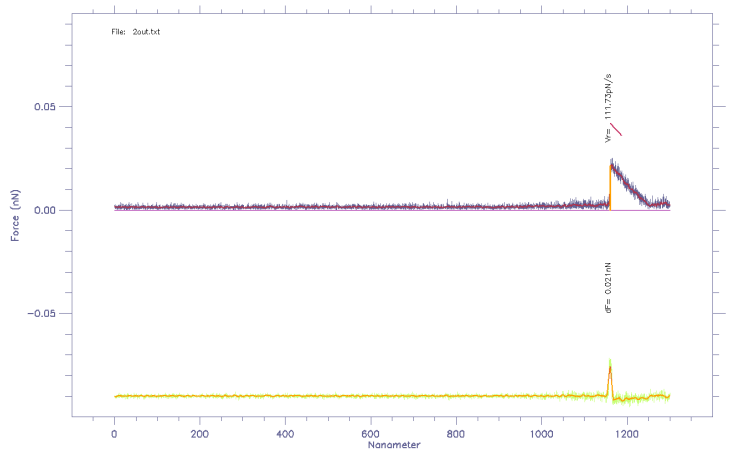

(b)

Figure 2.2.2: *(a)* Illustration of the procedure used to determine the rupture forces, their loading rate, and distances from the contact point (green triangle) for different experimentally observed force jumps from AFM by use of softeware developted by Professor Bjørn Stokke (named difordijpkv31d). The force retraction curve is shown in blue, -and its derivative in green. The force retraction curve shown was obtained when retracting an AFM tip functionalized with MUC1-ST from a mica surface functionalized with Gal3. *(b)* Illustration of the procedure used to determine the rupture forces and their loading rate for different experimentally observed force jumps from OT by use of the software developed by Professor Bjørn Stokke (named iNanoTrackerPostProcess2). The force curve is shown in blue, -and its derivative in yellow. The force retraction curve shown was obtained when a MUC1-ST functionalized polystyrene bead was forced to interact with a Gal3 functionalized polystyrene bead.

Chapter 3

Results

3.1 Typical interaction curves

Interactions between MUC1-ST and Gal3 were investigated by AFM force measurements and compared to interactions between MUC1-T and Gal3, which was the positive control. A few negative control experiment were also performed: interaction between MUC1-Tn and Gal3, interaction between MUC1-Naked and Gal3, a mucin with no glycans attached, MUC1-ST and-T and a silinazed mica surface, and a silianised AFM tip and Gal3, all expected to not give rise to any specific interactions.

Frequent interactions were observed for Gal3 when interacting with MUC1-ST, slightly less frequent interaction was observed for Gal3 and MUC1-T, and even less frequent interactions were observed for the negative control experiments.

Force retraction curves containing signature of force rupture were obtained for interaction between Gal3 and MUC1-T, -ST and to some extent -Tn, -Naked, and silanized mica without MUC1. Examples of these are depicted in Figure 3.1.1 and Figure 3.1.2. On the x-axis is the piezo-retraction distance, between the cantilever and the probe surface. MUC1-ST and -T gave no signature interaction events when probed against silanized mica.

The grey curve represents the approach by the cantilever to the surface, beginning from the left, and is deflected away from the surface as the cantilever and surface come in contact. The colored curve represents the retraction of the cantilever, and any deviation from the approaching curve represents deflection of the cantilever due to interaction forces acting between the two molecules. The last peak (to the right) represents the last interaction rupturing. The distance from the peak to the approach curve (base line) represents the force required to rupture the interaction, and the slope

leading up to the rupture is the associated loading rate (N/s).

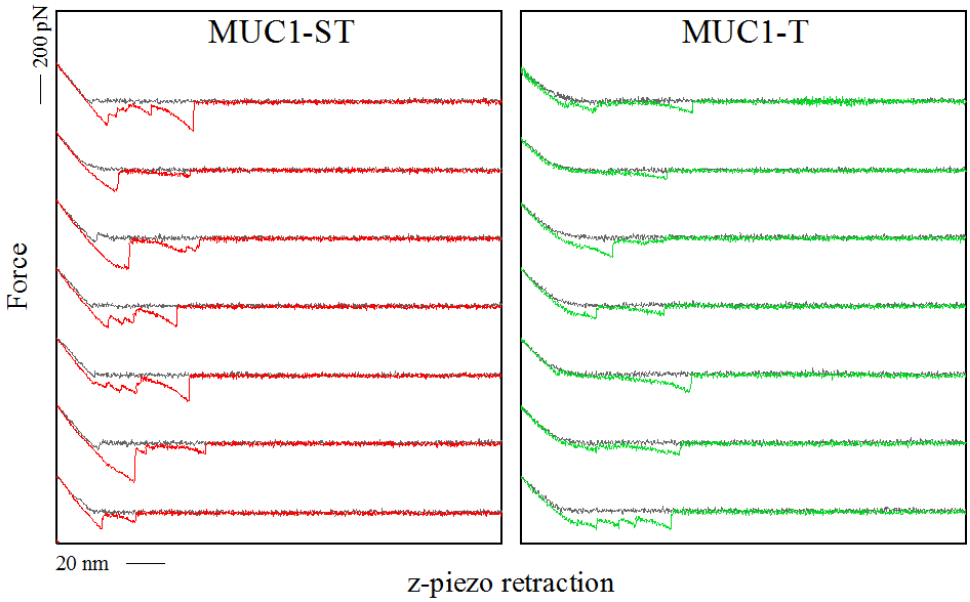

Figure 3.1.1: Gallery showing typical interaction signature events obtained by AFM for interaction between Gal3 and MUC1-ST, and -T. The inter-molecular curves were obtained using a retraction speed equal to 0.5 µm/s.

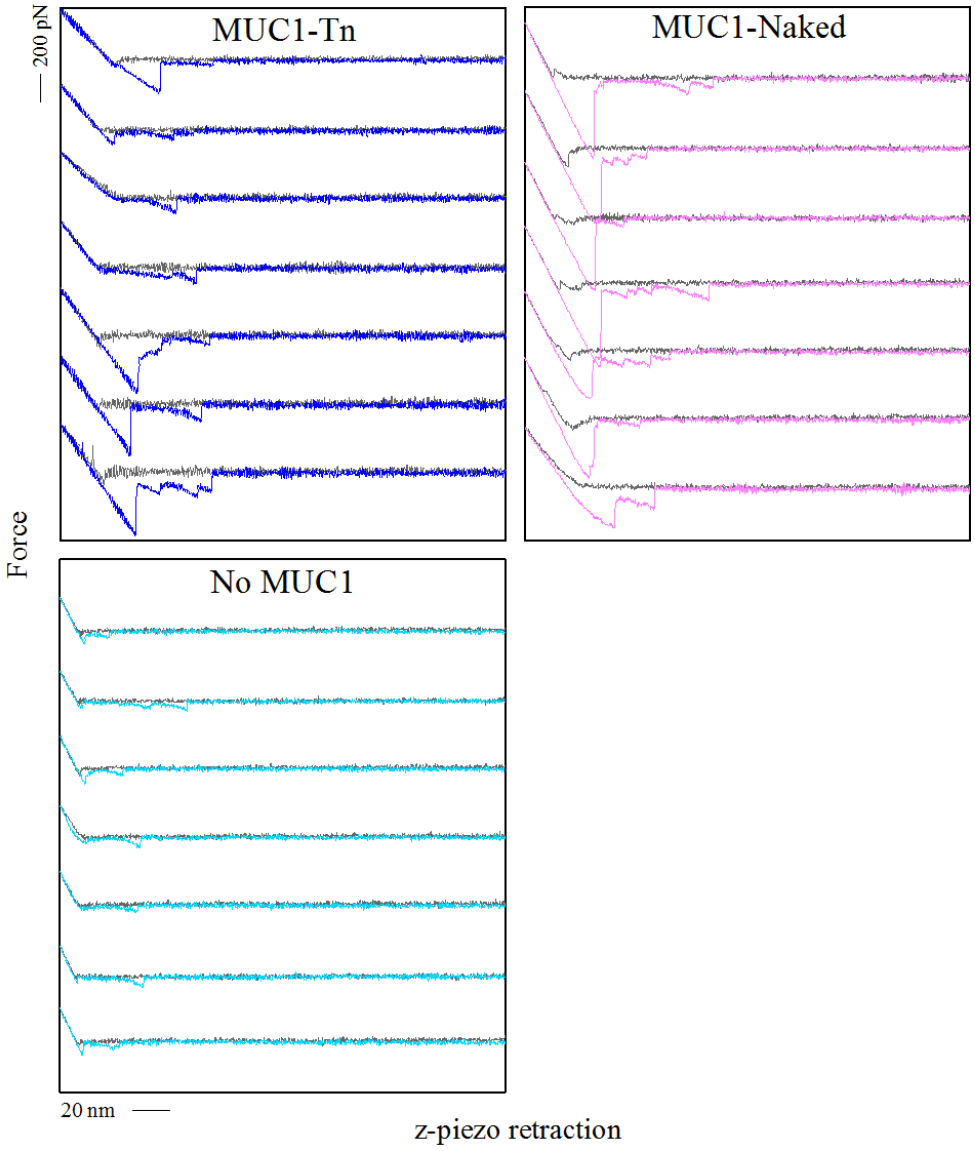

Figure 3.1.2: Gallery showing typical interaction signature events obtained by AFM for interaction between Gal3 and MUC1-Tn, MUC1-Naked, and between Gal3 and silanized cantilever (labelled No MUC1 in the figure). The inter-molecular curves were obtained using a retraction speed equal to 0.5 and µm/s.

3.2 Frequency of signature interaction events

The amount of force curves containing signature interaction events, as well as the number of curves not containing such events were determined. Figure 3.2.1, as well as Table 3.2.1, presents the result of this analysis for experimental series obtained for interactions between MUC1-ST, -T, –Tn, -Naked and Gal3, and between silanized cantilever without MUC1 interacting with Gal3, and MUC1-ST and -T interacting with silanized mica slide without Gal3. A breakdown of the data into different experimental series for interactions between MUC1-ST, -T and, -Tn with Gal3 was conducted to highlight variations from one experimental series to the next, and is presented in Table 3.2.2.

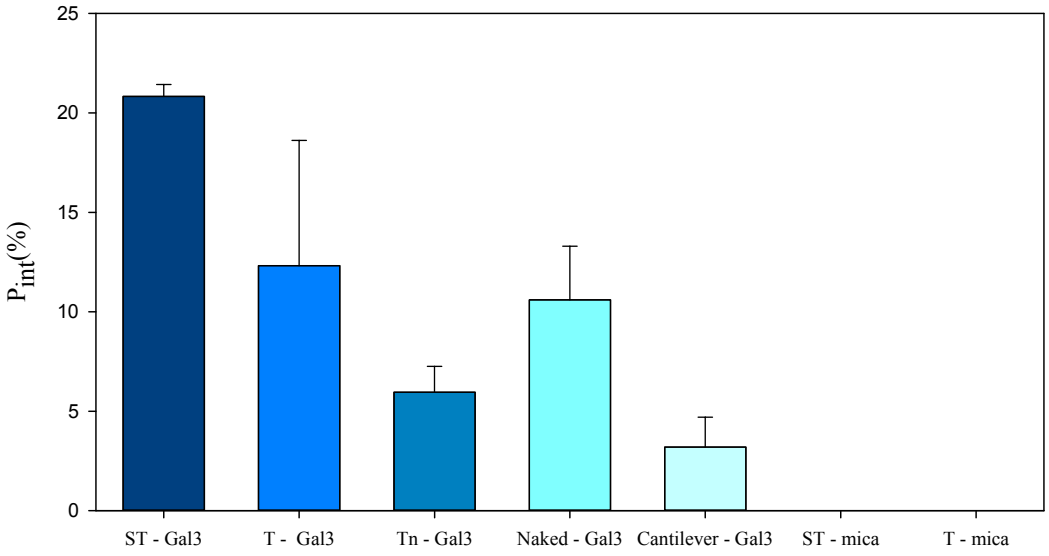

Figure 3.2.1: Frequency of curves containing signature interaction events for interaction between Gal3 and MUC1-ST, -T, -Tn, -Naked, and silanized cantilever, and between silanized mica and MUC1-ST and -T. Because of the large size variations, the interactions are calculated based on the nine last experimental series, with the three most high and low series excluded. The histogram is summarized in Table 3.2.1. The makeup of each bare is explained in Table 3.2.2. All AFM tips with immobilized MUC1 were prepared with an incubation concentration of 0.2 mg/ml MUC1 and about 1.5 mg/ml EDC, allowed to incubate for 45 minutes. All Gal3 covered mica slides was prepared using freshly cleaved, silanized mica, with a incubation concentration of 0.01 mg/ml Gal3 and about 1.5 mg/ml EDC.

Table 3.2.1: Fraction of force curves containing signature reflecting rupture of intermolecular interaction, P_{int}, obtained for MUC1-ST, -T, -Tn, -Naked, and silanized cantilever interacting with Gal3, and for MUC1-ST and-T interacting with silanized mica. The standard deviation (SD) was estimated for each P_{int}

Glycan	$\mathbf{P_{int}}$	**SD**
ST	20.8	0.6
T	12	6
Tn	5	1
Naked	10	3
Cantilever	3	1
ST-mica	-	-
T-mica	-	-

Table 3.2.2: Fraction of force curves obtained for MUC1-ST, -T, -Tn -Naked and silanized cantilever interacting with Gal3, and for MUC-ST and -T interacting with silanized mica, containing signature reflecting the rupture of inter-molecular interaction event, for different experimental series making up the basis for the interaction frequency analysis.

Glycan	**Series**	**P_{int} [%]**	**k [pN/m]**	**EDC [mg/ml]**	**v [m/s]**
ST	A	21.50	20	1.55	1.0
	B	20.50	18	1.55	1.0
	C	20.50	17	1.75	0.5
T	D	10.00	13	1.60	2.0
	E	20.00	11	1.60	0.5
	F	8.50	11	1.60	1.0
Tn	G	4.29	14	1.75	0.5
	H	6.00	21	1.75	1.0
	I	7.00	18	1.75	2.0
Naked	J	11.50	34	1.50	1.0
	K	7.00	36	1.50	2.0
	L	12.00	32	1.50	1.0
Cantilever	M	2.50	30	1.75	1.0
	N	3.01	34	1.75	1.0
	O	2.34	34	1.75	2.0
	P	5.47	34	1.75	0.5
ST-mica	Q	-	-	1.75	2.0
	R	-	-	1.75	1.0
	S	-	-	1.75	0.5
T-mica	T	-	-	1.75	2.0
	U	-	-	1.75	1.0
	V	-	-	1.75	0.5

In an attempt to depict the different interaction characteristics of Gal3 with MUC1-ST and -T, and Gal3 with MUC1-Tn, a more detailed analysis of the curves was performed. For each rupture event, the distance from the contact point to where the rupture occurred was obtained. The result of this analysis is presented in Figure 3.2.2.

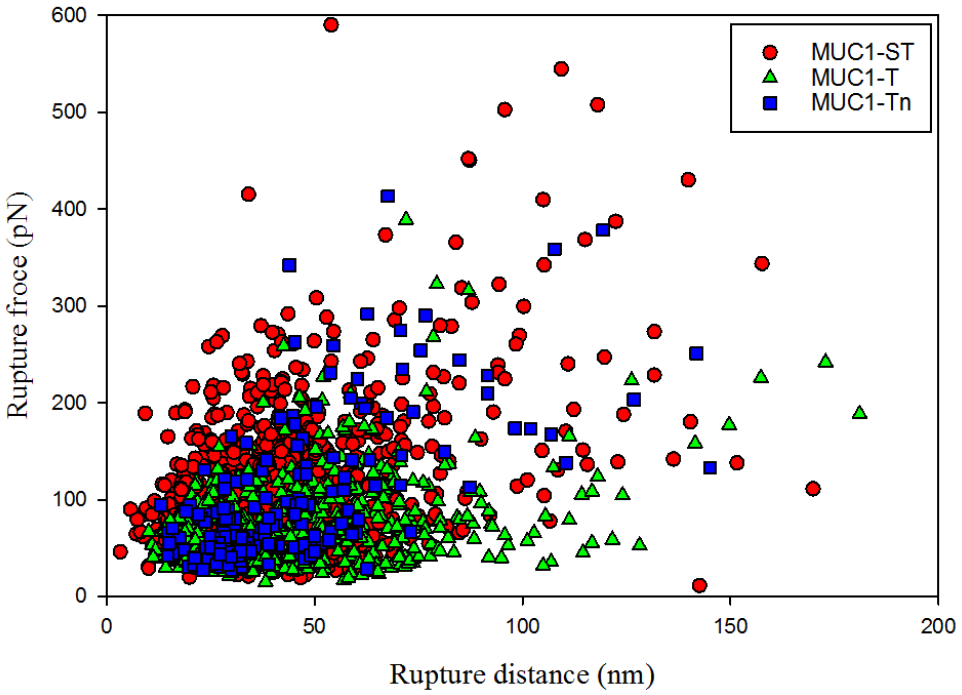

Figure 3.2.2: Rupture force (pN) for each separate force jump, with respective rupture distance (location of jump relative to the contact point, nm). Data from Gal3-MUC1-Tn experimental series are plotted together with data from Gal3-MUC1-ST and Gal3-MUC1-T interactions.

3.3 Imaging of mica slides with and without Gal3

Silanized mica slides and mica slides functionalized with Gal3 were imaged using tapping mode AFM. The instrument MultiMode8 was used, and Figure 3.3.1 depicts some of the images obtained.

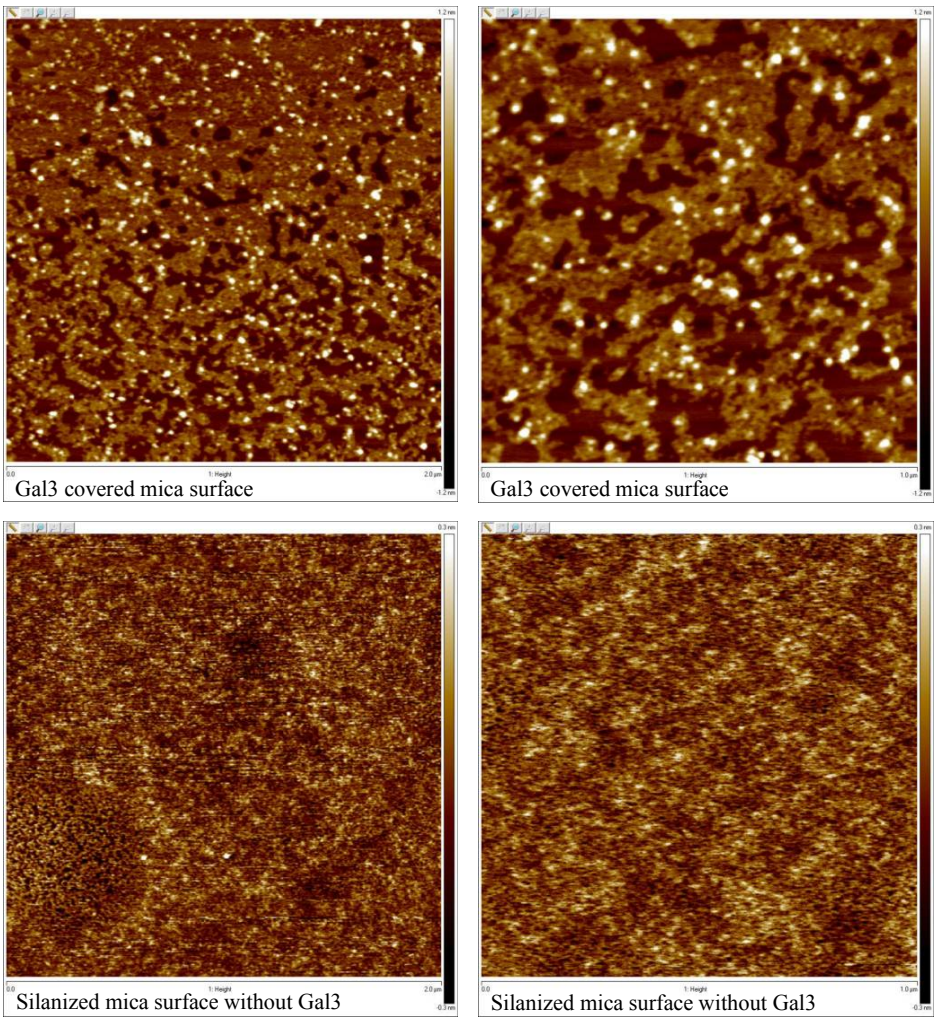

Figure 3.3.1: Two AFM images of a Gal3 covered mica slide, as well as images of a silanized mica slide. The two left images depicts a 2 by 2 µm section of the sample, the two to the right depicts a 1 by 1 µm section of the sample. Note that the color scale is different for the silanized samples and the samples functionalised with Gal3; highest (and lightest color) on the Gal3 functionalized mica represent 1.2 nm high peaks, highest (and lightest color) on silanized mica represent 0.3 nm peaks.

As shown in Figure 3.3.2, a profile from a selected cross-section of a mica slide with Gal3 containing peaks was selected in order to visualize the height differences accross the surface. Both the image where the cross-section was selected from, and a graph of the section is depicted in Figure 3.3.2. The graph correspondes to the height variations along the white line that is overlayed on the AFM image.

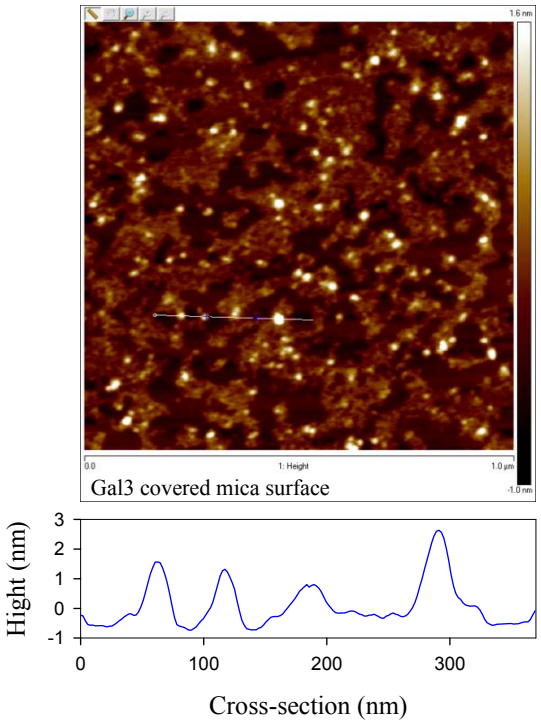

Figure 3.3.2: A cross-section of a Gal3 studded mica slide containing peaks was investigated using the NanoScope Analysis (version 1.40) and the height profile was plotted. The Gal3 studded mica slide was prepared as described in Chapter 2, section 2.2.1.

As it was observed that some of the area of the Gal3 mica surface seemed flat, a height profile of this was compared to a profile of the mica slide without Gal3. This comparison is depicted in Figure 3.3.3. Again, the graphs corresponds to the height variations along the white line overlayed on the images.

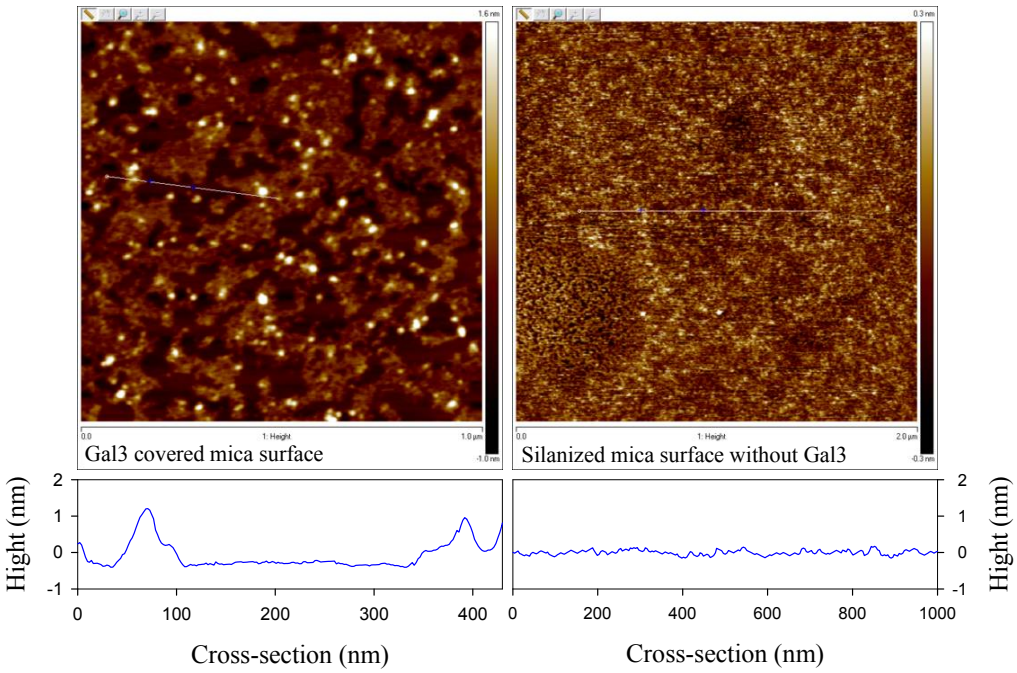

Figure 3.3.3: The left panel displays a scan of a Gal3 covered mica slides, and a cross-section containing what seemed to be a relative flat area. The right panel displays a scan of a silanized mica slide with a random crosssection selected. Both samples was silanized as described in Chapter 2 Materials and Methods, section 2.2.1 and the Gal3 samples was immobilized also as described there.

A roughness analysis of the two images showed in Figure 3.3.3 was performed using the software NanoScope Analysis (version 1.40), and the result is presented in Table 3.3.1. In addition, a roughness analysis was also performed on a section of the flat area observed on the Gal3 sample, and investigated in Figure 3.3.3, and a similar sized section of the silanized sample, presented in Table 3.3.1 as Gal3_{flat} and Silanized_{flat}.

3.4 MUC1-T interactions

Figure 3.4.1 presents the result of the initial analysis for MUC1-T-Gal3 interactions. The different rupture forces are plotted against associated loading rate. To determine the most probable force observed at a given loading rate, the observations were divided into ten subsets of loading rate intervals. A histogram for each subset was used to determine most probable force. All associated histograms are presented in Appendix A, page 75.

Table 3.3.1: R_a, the average roughness, was determined for both a Gal3 covered mica slide and a silanized mica slide, prepared as described in Chapter 2 Materials and Methods. The parameter was obtain using the NanoScope Analysis software (version 1.40).

Sample	R_a **(nm)**
Gal3	0.2540
Silanized	0.0706
Gal3_{flat}	0.0410
Silanized_{flat}	0.0516

From the analyses, x_β was determined based on the linear regression of the dynamic force spectrum. The lifetime, τ_0, and the most probable rupture force, f^*, was determined for each loading rate interval and the parameters are presented in Table 3.4.1. The mean dissociation coefficient was calculated as $\overline{k_{off}}$= 4 s^{-1}, corresponding to a mean lifetime of the biomolecular complex to be τ_0=0.25 s, when excluding the last four intervals, which lacked sufficient amount of data for good determination of parameters. Note that x_β and $\overline{k_{off}}(0)$ also could be calculated from a fit of Equation 1.6.9 to a plot of f^* versus $ln(r_f)$.

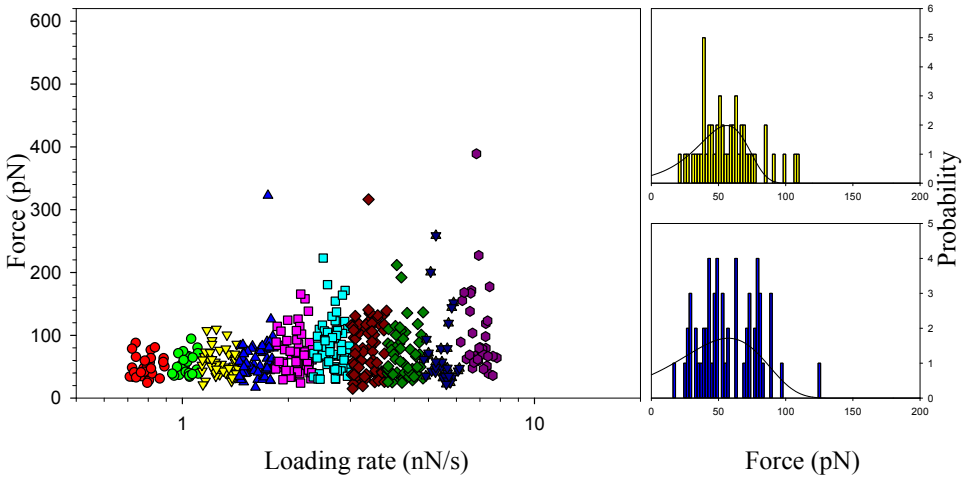

Figure 3.4.1: Steps in the analysis of the MUC1-T interaction with Gal3: Scatterplot of experimentally determined force rupture events of MUC1-T-Gal3 interaction in increasing force loading rates. The use of different tip retraction speeds and determination of the loading rate for each force jump, resulted in a continuously increasing distribution of unbinding forces as a function of increasing loading rate. The data are collected using a tip retraction speed of 2, 1, and 0.5 µm/ s. Based on the determined loading rate, the continuous distribution of observations was divided into ten subgroups characterized by a mean loading rate. Histograms based on the observed unbinding forces within each subgroup were generated, and the lifetime, τ_0 , as well as the most probable rupture force was determined for each subgroup. The fitted lines, from which the parameters f^* and k_{off} are obtained, are overlaid on the distributions presented. All associated histograms are displayed in Appendix A, page 75.

Table 3.4.1: Parameters charactering the energy landscape of Gal3-MUC1-T interactions determined from the data in Figure 3.4.1 above. The four last intervals were determined to not hold sufficient amount of data for determination of the parameters.

Interval	**N**	r_f **[pN/s]**	k_{off} **[1/s]**	x_β **[nm]**	f^* **[pN]**
1	31	787	5	0.20	43
2	25	1031	4	0.20	51
3	49	1296	4	0.20	56
4	59	1640	4	0.20	63
5	60	2103	5	0.20	62
6	76	2663	3	0.20	80
7	74	3350	17	0.20	46
8	51	4257	25	0.20	43
9	30	5466	69	0.20	-
10	35	6962	50	0.20	33

3.5 MUC1-ST interactions

Figure 3.5.1 depicts the result of initial analysis for MUC1-ST-Gal3 interactions, the different rupture forces are plotted against associated loading rate. To determine the most probable force observed at a given loading rate, the observations were divided into nine subsets of loading rate intervals. A histogram for each subset was used to determine most probable force. All histograms are depicted in Appendix A, page 75.

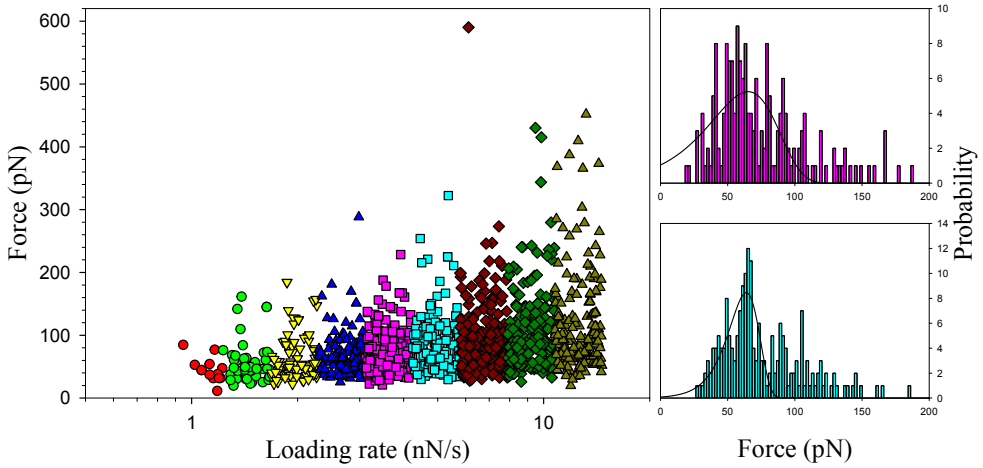

Figure 3.5.1: Steps in the analysis of the MUC1-T interaction with Gal3: Scatterplot of experimentally determined force rupture events of MUC1-T-Gal3 interaction in increasing force loading rates. The use of different tip retraction speeds and determination of the loading rate for each force jump, as described in the text, resulted in a continuously increasing distribution of unbinding forces as a function of increasing loading rate. The data are collected using a tip retraction speed of 2, 1, and 0.5 µm/ s. Based on the determined loading rate, the continuous distribution of observations was divided into nine subgroups characterized by a mean loading rate. Histograms based on the observed unbinding forces within each subgroup were generated, and the lifetime, τ_0 , as well as the most probable rupture force was determined for each subgroup. The fitted lines, from which the parameters f^* and k_{off} are obtained, are overlaid on the distributions presented in. All associated histograms are displayed in Appendix A, page 75.

From the analyses, x_β was determined based on the linear regression of the dynamic force spectrum. The lifetime, τ_0, and the most probable rupture force, f^*, was determined for each loading rate interval and the parameters are presented in Table 3.5.1. The mean dissociation coefficient was calculated as $\overline{k_{off}}$= 8 s^{-1}, and the mean lifetime of the interactions was calculated as τ_0=0.125 s. Note that x_β and $\overline{k_{off}}(0)$ also could be calculated from a fit of Equation 1.6.9 to a plot of f^* versus $ln(r_f)$.

Table 3.5.1: Parameters charactering the energy landscape of Gal3-MUC1-ST interactions determined from the data in Figure 3.5.1 above.

Interval	**N**	r_f **[pN/s]**	k_{off} **[1/s]**	x_β **[nm]**	f^* **[pN]**
1	13	1128	7	0.21	40
2	535	1463	7	0.21	45
3	89	2004	8	0.21	49
4	131	2750	7	0.21	58
5	183	3628	7	0.21	64
6	204	5012	8	0.21	66
7	251	6728	5	0.21	80
8	222	9100	10	0.21	74
9	190	12 512	11	0.21	79

3.6 Comparison of interactions between Gal3 and MUC1-ST, and –T

Figure 3.6.1 presents the most probable force, f^*, for different loading rates for MUC1-T and MUC1-ST in interaction with Gal3. The most probable force was determined by fitting Equation 1.6.8 to each histogram from the original scatterplots (Figure 3.4.1 and 3.5.1). The two datasets overlap. They show similar rupture forces and loading rates, as well as similar relationship between rupture force and loading rate. For MUC1-T - Gal3, f^* for the last four intervals was excluded as these intervals did not contain enough data so parameters could be determined correctly. Note that the error bars were calculated as standard deviations of the mean of the data contained in each bin of loading rates, and not as the fit of Equation 1.6.8 to the distributions.

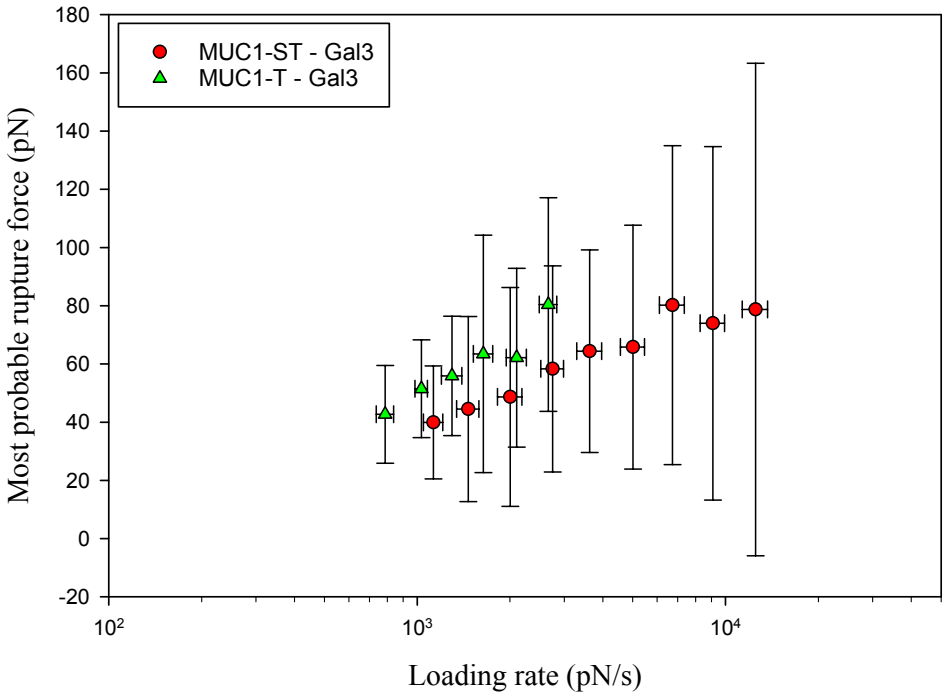

Figure 3.6.1: Most probable rupture force plotted against loading rate for Gal3-MUC1-T and Gal3-MUC1-ST, obtained by AFM using a retraction speed of 2, 1 and 0.5 µm/s. The two datasets overlap. They show similar rupture forces and loading rates, as well as a similar relationship between them. The most probable rupture force from the four last intervals for MUC1-T - Gal3 interaction was not included, as their associated histograms was not suitable for fitting of Equation 1.6.8. Note that the error bars were calculated as standard deviations of the mean of the data contained in each bin of loading rates, and not as the fit of Equation 1.6.8 to the histograms.

3.7 Comparison between OT and AFM data

Figure 3.7.1 shows the interactions between Gal3 and MUC1, obtained from OT and AFM. Data obtained using OT lies in the range of 0 to 50 pN, while the data obtained from AFM mostly lies in the range of zero to 200 pN. The loading rates also differs in the two datasets, data obtained from OT ranges from 10 to 110 pN/s, while data from AFM ranges from 1,000 to 100,000 pN/s. A gallery of the typical interaction events is depicted in Figure 3.7.2.

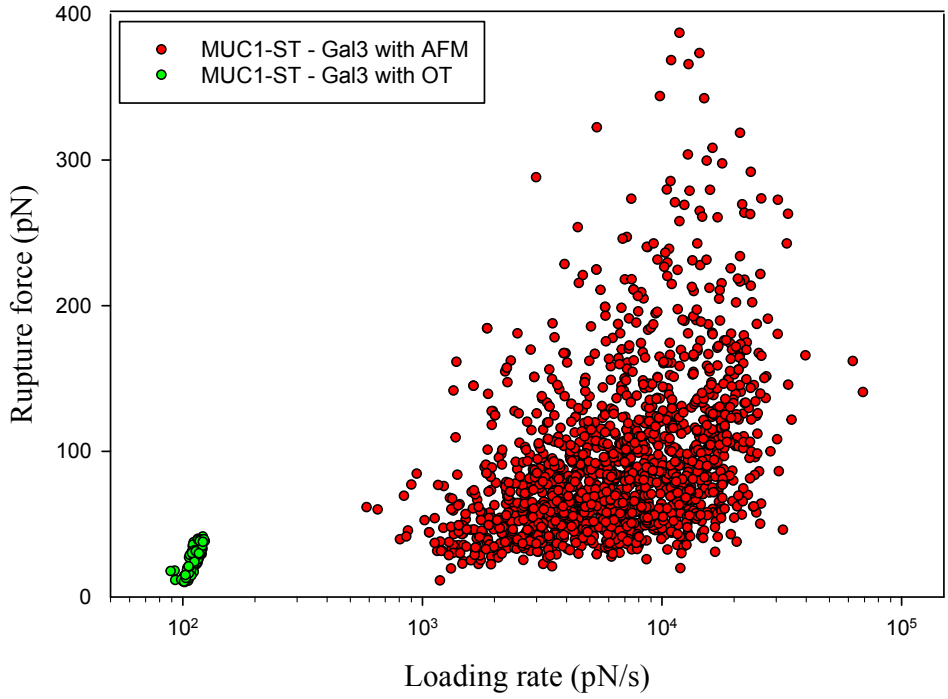

Figure 3.7.1: Comparison of data obtained using AFM and OT for MUC1-ST-Gal3 interactions. Preparation of samples as described in Chapter 2 Materials and Methods. The data from the OT contains 1607 force ruptures, while the data from OT only contains 103 force ruptures.

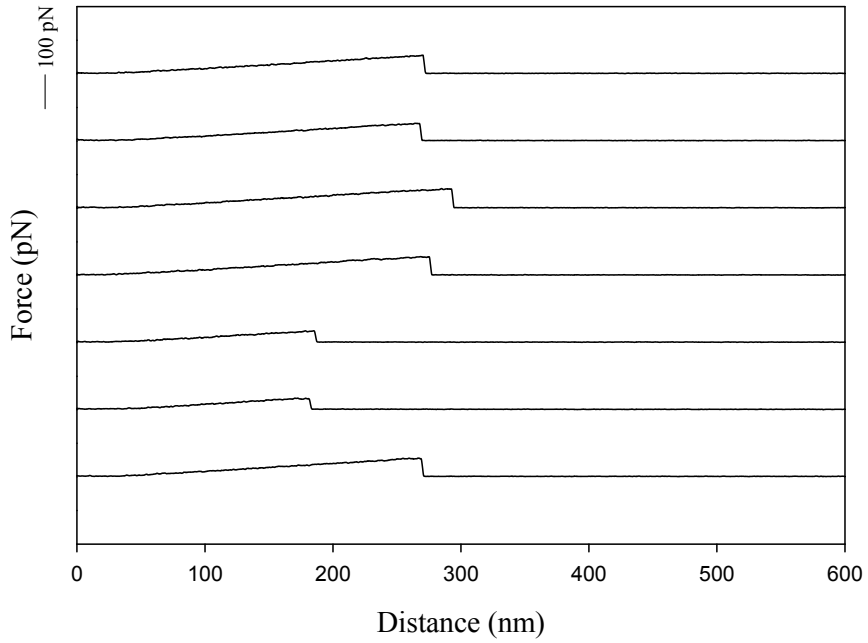

Figure 3.7.2: A gallery showing typical interaction curves obtained using the OT for interactions between MUC1-ST and Gal3.

Chapter 4

Discussion

The results show that MUC1-ST interacts with Gal3 in a similar way as MUC1-T. The results also show that there is a difference between the interactions observed between Gal3 and MUC1-ST and the negative control experiments.

4.1 Typical interaction events from AFM

The typical curves from AFM measurements of the interaction between Gal3 and MUC1-ST and -T, is presented in Figure 3.1.1. These suggests that molecular interaction occasionally form when the molecules are forced together. Some of the interaction events seems to exhibit the characteristics of a multiple interaction, where the different force jumps are not well separated (the retraction curve between the jumps doesn't reach the base line). This may suggest that multiple Gal3 are interacting with a MUC1 tandem repeat with multiple binding sites, or that multiple Gal3 are interacting with several MUC1. Several of the force curves exhibit a typical saw-tooth structure as described for receptor-ligand interaction with multiple binding sites[40, 42]. Interaction between Gal3 and MUC1-T and -ST was thus confirmed, but surprisingly rupture events were observed also for Gal3 functionalized surfaces interacting with MUC1-Tn and MUC1-Naked functionalized AFM tips, which were used as negative controls.

4.2 Frequency of signature interaction events and negative control experiments

To verify the main hypothesis that specific interaction occurred between MUC1-ST and Gal3, a positive control experiment and several negative control experiments where conducted. The frequency of signature interaction in each of these experiments is presented in Figure 3.2.1 Interaction between Gal3 and MUC1-ST was confirmed, but exhibited a higher frequency of interaction events compared to that of MUC1-T and Gal3. MUC1-ST probed against Gal3 had a 20.8% ± 0.6 interaction frequency, while MUC1-T probed against Gal3 had a frequency of 12% ± 6. As preliminary work conducted by Gianfranco Picco, King's Collage, London, indicated that Gal3 also showed specificity for MUC1-ST, and that in the presence of an inhibitor, LacNAc, MUC1-ST seemed to bind more avidly to Gal3 than MUC1-T, as presented in Figure 4.2.1b, this fits well with the trends observed here. This trend was also observed in a parallel experiment conducted by another master student, Øystein Haug, investigating the same proteins with optical tweezers (OT).

Although the negative control experiments all exhibited a lower interaction frequency than that of MUC1-ST, some of the experiments did not differ much from that of MUC-T, used in this study as the positive control. Especially, the experiment where MUC1-Naked was probed against Gal3, exhibiting a interaction frequency of 10% ± 3, was very close to the interaction frequency where MUC1-T was probed (12% ± 6). The MUC1-Naked sample used was purified using affinity chromatography, and should have no glycans prensent. The interaction observed could thus most likely not be attributed to impurities, but something else. This issue is discussed in more details under subsection 4.2.1

The frequency of interaction events analysis is based on a protein immobilization concentration optimised for dynamic force spectroscopy (DFS) analysis, and a larger difference between the behaviour of the different samples could possibly have been observed if experiments also were conducted with a higher density of MUC1 on the AFM tip, as seen in Beatson *et. al.* [13]. In this study, where interactions between MUC1 and the macrophage galactose-type C-type lectin (MGL) was investigated, a greater difference between interaction frequency of positive and negative control was observed when a higher MUC1 density was used. This would be in accordance with reports that the frequency of interaction is concentration dependent[11], hence a higher density of MUC1 would produce more frequent specific interaction events.

A possible solution to further strengthen the hypothesis of specific interaction between

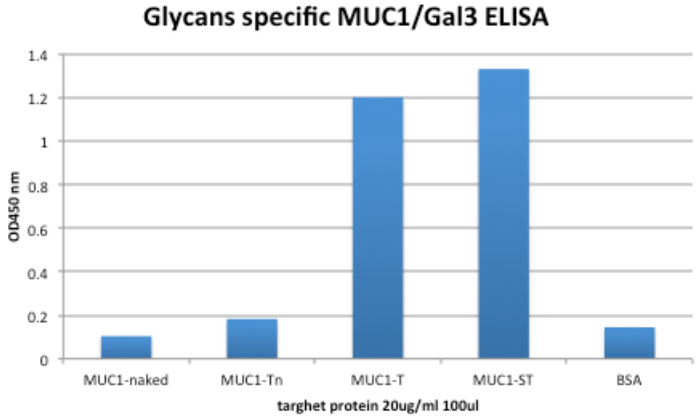

(a)

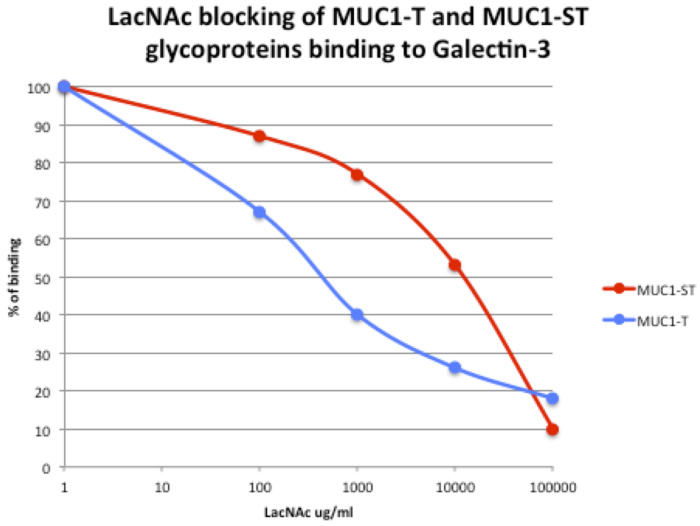

(b)

Figure 4.2.1: Preliminary work conducted by Gianfranco Picco, King's Collage, London. (a) Recombinant MUC1 glycoproteins expressing predominantly either no O-linked glycans or the glycan Tn, T or ST were used as target protein by coating ELISA plates with 2 µg of proteins, before blocking with BSA, Gal3 binding and colorimetric visualization. (b) LacNAc blocking of MUC1-T or -ST /Gal3 binding: Recombinant Galectin 3 was used as target protein by coating ELISA plates with 2 µg O/N. The coating was followed by 1 hour blocking with 2% BSA before the use of MUC1 glycoproteins expressing predominantly either the glycan, T or ST with an increasing concentration of LacNAc and colorimetric visualization. Both graphs provided by Gianfranco Picco, King's Collage, London.

Gal3 and MUC1-ST could be to use an inhibitor, such as LacNAc or Galactose to the solution, so that binding sites on Gal3 would all be occupied, thus resulting in a lower frequency of interactions.

4.2.1 Influence of glycosylation on MUC1 structure and persistence length

Although there are some variation of measured persistence length of human mucins in solution (varying between 10[57] and 36 nm[58, 59]), there is great consensus that the rigidity and wormlike polypeptide characteristics of MUC1 are due to steric hindrance between the O-linked glycans[59, 60]. Shogren *et. al.*[60] found that when glycans where removed from MUC1, the rigid structure and long persistence length collapsed, and that the protein now exhibited a structure typical for that of denatured globular proteins. This is critical for the experiment where MUC1-Naked was used, MUC1-Naked has no glycans, and would thus be expected to hold this collapsed structure. This is likely to affect the frequency of non-specific interaction when using AFM. The shortened persistence length of the mucins can allow for more non-specific interaction between the silanized AFM tip and the surface coveres with Gal3, and the collapsed structure of MUC1 could allow for non-specific interactions between parts of the polypeptide backbone otherwise shielded by the glycans. It could be argued that the MUC1 polypeptide backbone acts as a linker between the AFM tip and the O-linked glycans, decreasing the chances of non-specific interaction between cantilever and Gal3 covered mica slide. This also accounts for the interactions observed for MUC1-Tn and Gal3 (5% ± 1), as the Tn glycan is an oligosaccharide, shorter that T and ST, and therefor expected to also exhibit a more collapsed structure. Shogren *et. al.*[60] reported that mucins with two or more carbohydrate residues per side chain experienced a three-fold expansion in dimensions (MUC1-T have two carbohydrate residues per side chain, ST has thee).

If the above explanation holds some truth, the interactions observed between MUC1-ST and -T with Gal3 should consist of less non-specific interactions than what the negative control studies suggests. They are not expected to included the non-specific interactions observed for the negative control experiments, as these would decrease as the stiffness and persistence length of the MUC1 increases. Additional control experiment with MUC1-Naked and silanized mica would thus be very interesting , as this explanation suggest that non-specific interactions also might occur for this system. Because of limited time, such an experiment was not prioritized. Because of the different structure/persistence length of MUC1-Naked compared to MUC1-ST and -T, one could argue that this control experiment is misleading and should be disregarded.

4.2.2 Rupture distance analysis

In an attempt to highlight possible differences in the distance of the rupture events in relation to the contact point, a plot of rupture distance versus rupture force was made for interactions between Gal3 and MUC1-ST, T and Tn, as depicted in Figure 3.2.2. However, this plot did not reveal any different trends, as most rupture events for all the systems investigated were clustered in the same area. This analysis could reveal such differences if a linker was used between the proteins and the surfaces, as this would increase the distance between the specific inter-molecular rupture events and the non-specific interactions concentrated near the contact point, making it easier to distinguish them.

4.3 Immobilization and density of Gal3 on mica surface

In AFM experiments, one wishes to obtain a consistent and dense cover of the selected protein on the mica surface. This could be achieved in multiple ways as the molecule density may be affected by several factors. Those include the effectiveness and concentration of EDC, the cross linker, incubation time and temperature, and concentration of the selected molecule in the immobilization solution. EDC is stored at -18°C, and is expected to loose effectiveness over time, especially if exposed to higher temperatures, and if absorbing moisture from air while being opened. As the effectiveness of EDC decreases drastically after being dissolved at room temperature, it's far more effective in the beginning of the incubation period, hence incubation time may not affect the molecular density on prepared samples as much as one would expect. In the current study, a fixed concentration of EDC was used, but due to the electrostatic behaviour of the solid EDC during weighting, some inaccuracy is expected, altering the concentration used during the immobilization step. The chemical reaction of cross linking, and the effectiveness of EDC, are both temperature dependent, and after feedback (Associate Researcher Gianfranco Picco, King's Collage, London, 2016 [pers.comm.]) all incubations was performed on ice.

A surface topography image of a prepared Gal3 covered mica slide was obtained using a scanning AFM (MultiMode8), and compared to a similar image of a silanized mica slide, as presented in Figure 3.3.1. The images clearly shows that proteins are immobilized inter-molecular the mica slides, and this was further confirmed by a height profile analysis performed and depicted in Figure 3.3.2. The associated graph reveal peaks of about 2-3 nm, consistent with the radius of a spherical protein with a molecular weight of 29-35 kD, like Gal3 (R_{min} ranging from 2.03 nm to 2.16 nm, calculated as described

in Erickson, 2009[61]).

The roughness parameter, R_a, displayed in Table 3.3.1 for a Gal3 covered mica sample (0.253 nm) and a silanized mica sample (0.0706 nm), clearly shows that proteins were immobilized on the mica surface as desired.

A height profile from the flat area seen on the Gal3 sample was compared to a height profile from the silanized sample, Figure 3.3.3. This comparison clearly reveal that the flat area on the Gal3 surface is as flat as the silanized sample, also confirmed by the similar R_a values diplayed in Table 3.3.1 on page 44 (0.0410 nm for the flat area on the Gal3 sample and 0.0516 on a similar sized area on the silanized sample). Thus it is clear that the Gal3 covered surface is not very densely covered by Gal3, increasing the possibility that the AFM tip could encounter no Gal3 when in contact. The Gal3 image is approximately 1 by 1 µm and some of the flat areas spread 0.2 µm wide, and as the AFM measurements are set up as a 10 by 10 µm matrix with measurements every 1.0 µm, there is a chance that the AFM tip can be lowered inter-molecular a uncovered area of the Gal3 covered sample. This could lead to non-specific interactions between the silanized mica and the functionalized AFM tip, but is unlikely as the control experiments where MUC1- ST and -T was probed against a silanized mica surface gave rise to no interaction events. Thus, this not so dense cover of Gal3 on the mica slide would lead to less frequent interactions with MUC1-ST and -T, but no increase in non-specific interaction between the mucins and the uncovered silanized area. The not so dense cover of the surface could also explain the variations observed in the frequency analysis, where standard deviations is as high as ±6% for the MUC1-T - Gal3 experiments.

4.4 Correlation between OT and AFM data

In Figure 3.7.1, the force and loading rate is plotted for MUC1-ST - Gal3 data obtained from the AFM studies presented, as well as data from OT. The experiments with the OT was conducted using a much higher protein immobilization concentration than that obtained after optimisation by another student conducting a parallel experiment. The OT data presented in Figure 3.7.1 exhibits a different relationship between rupture force and log loading rate than that of the AFM data. This could be explained by the mentioned high protein immobilization concentration, or the fact that the conclusion is not valid due to few data points in the dataset. OT data kindly provided by the mentioned student conducting a parallel experiment is depicted here in Figure 4.4.1. By ignoring the high force data from the OT most likely to represent multiple interactions, the remaining data corresponds in a linear way, as the Bell-Evans theory stipulates.

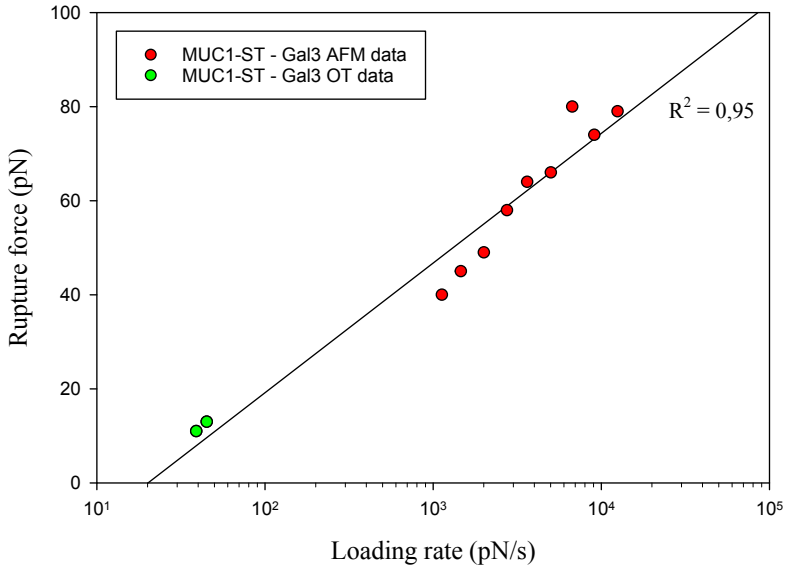

Figure 4.4.1: Comparison of data obtained using AFM and OT for MUC1-ST-Gal3 interactions, fitted by a linear regression. Preparation of samples for AFM experiments as described in Chapter 2 Materials and Methods. The data from the OT was kindly provided by another student conducting a parallel experiment, Øystein Haug and as he determined two energy barriers, only the data representing the inner barrier are presented here. The slope of the linear fit is 27.6, and this was determined by the use of linear regression in SigmaPlot.

The slope of 27.6 obtained after linear regression performed in SigmaPlot is equal to $(k_BT)/x_\beta$, after Equation 1.6.9, thus providing the opportunity to determine a new value for x_β. The new x_β based on both OT and AFM data was determined to be 0.15 nm, slightly lower than the obtained x_β for the AFM data of 0.21 nm. The estimation was performed using a value for k_B at 24 °C of 4.10 pN nm. The fit of the linear regression is good, and although the new x_β is lower than the one calculated based on the AFM data alone, this suggest similar results from the OT and AFM, strengthening the foundation of the obtained parameters. The OT data presented were kindly provided by another master student, Øystein Haug, conducting a parallel experiment. Only the data from the inner barrier was included, as the outer barrier possessed a much steeper slope, though to possibly be a result of high multiple characteristics.

4.5 Experimental noise and uncertainty in the parameters characterizing the energy landscape

Within the biochemical complex under investigation with AFM, several chemical bonds exists: both covalent bonds between Gal3 and the mica surface and MUC1 and the AFM tip, and (presumably) non-covalent bonds between the two proteins when they form a complex. Observed bond ruptures are most likely of the non-covalent type, as covalent bond is reported to range between one and 2twonN in strengh[62], and the observed ruptures mostly don't exceed 200 pN (0.2 nN).

The observed ruptures could stem from unfolding of protein. This is unlikely for MUC1, as MUC1 already exists in a rigid and unfolded structure. Gal3 is a globular protein, which would unfold if denatured, but this is unlikely, as experiments where Gal3 was probed against a silanized AFM tip resulted in an interaction frequency of 3% ±1. What is interesting, is that as MUC1-Naked contains no glycans, and therefor is likely to hold a very different structure than MUC1-ST and -T, unfolding of this protein is more likely.

4.5.1 Multiple interaction and AFM

When applying the Bell-Evans framework, one assumes that single interactions are studied, and that the energy landscape only contains sharp and harmonic wells. This might very well not be the case for dissociation of MUC1-Gal3 complexes. If Gal3 exists in a pentamer shape, as suggested by the literature, each pentamer would have more than one possible binding site for appropriately glycosylated MUC1. Each MUC1

molecule also has more than one glycan attached, so this can also interact with multiple Gal3s. This strongly suggests a high likelihood for multiple interactions, and is further strengthened by the tails in the histograms. The simple Bell-Evans framework may not be suitable for this investigation. If methods developed for the determination of energy landscape parameters for such complex inter-molecular interactions were implemented, this AFM study would be more suitable for this study. The multiplicity character of the system investigated is evident in the histograms as tails.

4.5.2 BSA

In an attempt to lower the multiplicity in the force versus retraction curve characterizing the MUC1-Gal3 system, a spacer molecule was used when preparing the the Gal3 covered mica slide. The Gal3 was immobilized inter-molecular the silanized mica surface with Bovine serum albumin, BSA, in a 25/75 ratio. This did not work as intended, as both the frequency of interactions and the multiplicity of the force versus retraction curves increased drastically. Some of the obtained force versus retraction curves are displayed in Figure 4.5.1. As this attempt failed, no investigation into why this happened was conducted, but this could be the attributed to interaction between BSA and MUC1 and BSA interacting with the AFM tip or some kind of unfolding events.

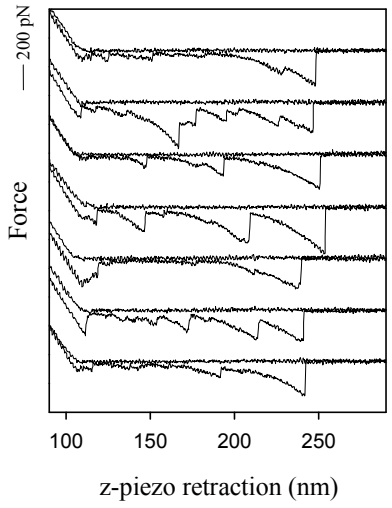

Figure 4.5.1: Gallery showing typical interaction signature events obtained by AFM for interaction between Gal3 and MUC1-ST when BSA was used as a spacer molecule on the Gal3 covered mica surface. The inter-molecular curves were obtained using a retraction speed equal to 1 µm/s.

4.6 Energy landscape of MUC1-T

In Figure 3.4.1, the force-loading rate data for interactions between MUC1-ST and Gal3 are presented, and divided into ten intervals along the axis of increasing loading rate. Two of the associated histograms are shown, presented with the fit of the equation for most probable loading force (Equation 1.6.8). These observations indicates a trend of increasing force with loading rate for the first sex intervals, in accordance with the theory (except for interval 4, which has a slightly higher (63 pN) mean force than interval 5 (62 pN)). The last four intervals indicate a trend of decreasing force with loading rate, and has a calculated dissociation coefficient more than four times than those of dissociation constants associated with the first six intervals. From the scatterplot in Figure 3.4.1, as well as the associated histograms presented in Appendix A, page 75 it seems that these intervals contains insufficient amount of datapoinst, and if more time was available, this should have been improved by performing more experiments. Each interval contain on average 49 datapoints, significantly lower than the 202 average for the MUC1-ST experiments. The dataset used in this type of analysis should ideally contain a lot of data, as a large dataset would maximize the accuracy of the fit, and the parameters determined. But as mentioned in the introduction, due to the stochastic nature of the system, and the multivalent nature of the proteins, a spread of forces is expected[44]. After most probable rupture force, $f*$, for each loading rate, r_f, was determined, and the linear equation for most probable loading force (Equation 1.6.9) was fitted, the parameters x_b, the dissociate rate k_{off}, and hence the lifetime, τ_0, was obtained.

For the MUC1-T-Gal3 interaction, the loading rate was ranging from 787 to 6962 pN/s, a bit lower than the reported range for AFM studies with MUC1 and lectins (about $10^2 - 10^5$ pN/s[54]). With a loading rate of 2663 pN/s, the most probable force was estimated to be 80 pN, about 2/3 of the reported values for MUC1-antibody interaction of 120 pN[63] (at a loading rate of 10^4 pN/s), and similar to reported unbinding forces reported for protein-ligand interactions[64], and unbinding forces associated with MUC1 heterotypical interactions[43].

The k_{off} is ranging from 3 s^{-1} to 5 s^{-1}, with a mean dissociation rate, $\overline{k_{off}}$, equal to 4 s^{-1} and an estimated lifetime of 0.25 s for the first six intervals. Reported k_{off} for the same MUC1-antibody interaction mentioned above was 2.6 x 10-3 s^{-1}[63], hence significantly lower than what was obtained here. Other studies of mucins have reported k_{off} = 0.76 ± 0.09 s^{-1}[25]. The lifetime, τ_0, of 0.125 s obtained is a bit lower than those reported for the heterotypical interactions between MUC1, ranging from 0.14-5.55 s[43]. The location of the energy barrier, x_β, was determined to be 0.20 nm away from the energy minimum, and is just within range of reported values for alginate complexes studied by AFM ranging from 0.2-0.5 nm[44].

All of the above point to a specific interaction between MUC1-T and Gal3 taking place, as expected, with reasonable determined parameters characterizing the energy landscape.

4.7 Energy landscape of MUC1-ST

In Figure 3.5.1 the force-loading rate data for interaction between MUC1-ST and Gal3 are presented and divided into nine intervals of loading rate. These observations indicate a trend of increasing force with loading rate, corresponding to the theory, except for interval 7, which has a slightly higher most probable rupture force (80 pN) than those of interval 8 and 9 (74 and 79 pN respectively). Two of the associated histograms are shown, presented with the fit of the equation for most probable loading force (Equation 1.6.8).

For the MUC1-ST-Gal3 interaction, the loading rate was ranging from 1128 to 12512 pN/s, closer to the reported typical range for AFM studies (10^4-10^5 pN/s) than the loading rates of MUC1-T-Gal3. The k_{off} is ranging from 5 s^{-1} to 11 s^{-1}, with a mean dissociation rate, $\overline{k_{off}}$ equal to 8 s^{-1} and a estimated lifetime, τ_0, of 0.125 s. Reported k_{off} for the same MUC1-antibody interaction mentioned above was 2.6 x 10-3 s^{-1}[63], hence significantly lower than what was obtained here. Other studies of mucins has reported k_{off}= 0.76 ± 0.09 s^{-1}[54]. The lifetime, τ_0 of 0.73 s obtained is within the range of those reported for the heterotypical interactions between MUC1, ranging from 0.14 - 5.55 s[43].

With a loading rate of 9100 pN/s, the most probable force was estimated to be 74 pN, just over half of the reported value for MUC1-antibody interaction of 120 pN[28] (at a loading rate of 10,000 pN/s), but similar to reported unbinding forces reported for protein-ligand interactions[29], and unbinding forces associated with MUC1 heterotypical interactions[20].

The location of the energy barrier, x_β, was determined to be 0.21 nm form the energy minimum, and is within the range of reported values for alginate complexes studied by AFM ranging from 0.2-0.5 nm[44].

4.7.1 Histograms associated with the DFS analysis

The obtained histograms for the DFS analysis, presented in Appendix A, page 75, all presents a single mode distribution, slightly skewed towards the right, typical for biomolecular complexes[52]. The absence of multiple peaks in the histograms contrast

the findings reported when biomolecular complexes containing multiple receptors or ligands are investigated. REF

4.8 Comparison of interactions between Gal3 and MUC1-T, and –ST

Most probable force, f^*, for the two different interaction types are plotted together in Figure 3.6.1. As the most probable rupture forces for the interaction between MUC1-T and Gal3 and MUC1-ST and Gal3 are in proximity of each other, and overlapping in the sense that they show similar rupture forces and loading rates, and a similar relationship between them. This indicates that the interaction between MUC1-ST and Gal3, and MUC1-T and Gal3, is very similar in strength and lifetime, further implicating a similar interaction mechanisms. Hence, the results indicate that MUC1-ST is a possibly new ligand for Gal3. Note that the error bars were calculated as standard deviations of the mean of the data contained in each bin of loading rates, and not as the fit of Equation 1.6.8 to the distributions. Because of the stochastic nature of bond rupture, and the multiple characteristic of the system studied, a spread in forces at a given loading rate is expected, thus resulting in large standard deviations. Alternatively, the vertical error bars could have been calculated based on the fit of Equation 1.6.8 to the associated histograms, thus rather reflect the *shape* of the distributions.

4.9 Future work

4.9.1 More data

As it might be be necessary to confirm the specificity of the MUC1-ST - Gal3 biomolecular complex, more data should be obtained for the positive control experiment with MUC1-T and Gal3. Furthermore, a higher Gal3 density can provide more reproducible experiment, with more consistent interaction frequencies. In addition to this, all experiments should also be conducted with a higher MUC1 concentration to hopefully obtain a more significant difference in the frequencies between the different MUC1 samples. It would also be interesting to see if the system behaves differently when a linker molecule is used, especially on the mica surface where Gal3 is immobilized, as MUC1 with attached glycans already accomplishes some of the properties of a linker, such as increasing the distance between the glycans and the cantilever surface. This would possibly result in a reduction of non-specific interactions.

From the obtained force versus retraction curves, a more accurate determination of parameters could be obtained by implementing new methods for dynamic force spectroscopy analysis. Such implementation could include confirmation of specific interaction events by searching for fingerprint frequencies in the curves as suggested by Bizzarri *et. al.*[52], by implementing development of the Bell-Evans framework regarding the effects of rebinding as suggested by Friddle *et. al.*[51], and/or by implementing improvements to the Bell-Evans framework made by Dudko *et. al.*[50]. The implementation of such new developments was not performed in this thesis due to limited time and resources.

In addition, it would be interesting to investigate the interaction between MUC1-ST and Gal3 on a cellular level, to possible confirm that the interaction occur, but also to confirm this interaction initiate the same intracellular processes and pathways as described in Chapter 1, Introduction, Section 1.3 Importance of Gal3-MUC1 interactions for cancer progression.

4.10 Importance of the findings

As both Gal3 and MUC1 are involved in metastasis[5, 15, 17] and development of cancer, through mutagenesis[15, 17] and oncogenesis[2] respectively, their function, both separately and together, may prove to be important for the treatment and diagnosis of cancer. Proving that Gal3 in addition to MUC1-T, also interacts with MUC1-ST when external force is applied, as with AFM and OT, this indicates that similar interactions take place also biologically, where no external forces are applied. The result indicates that the MUC1-Gal3 interaction might be more widespread and important than initially assumed. The results also provides a small contribution to the increasing research field surrounding glycobiology.

Chapter 5

Conclusion

The data presented in this thesis obtained by use of atomic force microscopy (AFM) shows that interactions between Gal3 and MUC1-ST occurred. A dynamic force spectroscopy (DFS) analysis revealed an energy landscape with rupture forces ranging between 40 pN and 80 pN at a loading rate interval of 1128-12512 pN/s. A single energy barrier was identified at x_β=0.21 nm, and $\overline{k_{off}}$ was estimated to 8 s^{-1}, corresponding to τ_0=0.125 s. These results were in good agreement with the results obtained when investigating the interactions between MUC1-T and Gal3, indicating that the properties of the Gal3 - MUC1-ST interactions are similar to those of the Gal3 - MUC1-T interactions. A good correspondence was also observed between data obtained using the alternative force probes optical tweezers and AFM in the sense that the data fell on the same straight line when taking both the rupture forces and the corresponding loading rates into consideration.

The fact that interaction events also occur between MUC1-ST and Gal3, similar to those known to occur between MUC1-T and Gal3, has implications of the understanding of the role of Gal3 and MUC1 for cancer progression and treatment. In the current study, some interaction events were also observed when the AFM tip was functionalized with MUC1-Tn and MUC1-Naked. This complicates the discussion since it opens for the interpretation that the interactions observed between MUC1-ST and Gal3, or a fraction of these, are non-specific. However, the similar characteristic of the interactions of the Gal3 - MUC1-ST complex and the Gal3 - MUC1-T complex, as observed using AFM and DFS, makes this interpretation unlikely.

Bibliography

[1] Donald W. Kufe. Functional targeting of the muc1 oncogene in human cancers. *Cancer Biology & Therapy*, 8(13):1197–1203, 2009. PMID: 19556858.

[2] Donald W. Kufe. Mucins in cancer: function, prognosis and therapy. *Nat Rev Cancer*, 9(12):874–885, 2009.

[3] Donald W. Kufe. Targeting the human muc1 oncoprotein: A tale of two proteins. *Cancer Biology & Therapy*, 7(1):81–84, 2008. PMID: 18347419.

[4] D W Kufe. Muc1-c oncoprotein as a target in breast cancer: activation of signaling pathways and therapeutic approaches. *Oncogene*, 32(9):1073–1081, 02 2013.

[5] Sritama Nath and Pinku Mukherjee. Muc1: a multifaceted oncoprotein with a key role in cancer progression. *Trends in Molecular Medicine*, 20(6):332–342, 2014.

[6] D. Kufe. Oncogenic function of the muc1 receptor subunit in gene regulation. *Oncogene*, 29(42):5663–5666, 2010.

[7] Claus Kordes, Iris Sawitza, and Dieter Häussinger. Canonical wnt signaling maintains the quiescent stage of hepatic stellate cells. *Biochemical and Biophysical Research Communications*, 367(1):116 – 123, 2008.

[8] Stefan Rudloff, Daniel Messerschmidt, and Rolf Kemler. Chapter 228 - wnt signaling in development. In Ralph A. Bradshaw and Edward A. Dennis, editors, *Handbook of Cell Signaling (Second Edition)*, pages 1873 – 1878. Academic Press, San Diego, second edition edition, 2010.

[9] Kazuaki Ohtsubo and Jamey D. Marth. Glycosylation in cellular mechanisms of health and disease. *Cell*, 126(5):855–867, 2006.

[10] J. Taylor-Papadimitriou, J. Burchell, D. W. Miles, and M. Dalziel. Muc1 and cancer. *Biochimica et Biophysica Acta (BBA) - Molecular Basis of Disease*, 1455(2–3):301–313, 1999.

[11] Robert S. Bresalier, James C. Byrd, Li Wang, and Avraham Raz. Colon cancer mucin: A new ligand for β-galactoside-binding protein galectin-3. *Cancer Research*, 56(19):4354–4357, 1996.

[12] R.D. Cummings A. Varki and J.D.Esko. *O-GalNAc Glycans*, book section 9. Cold Spring Harbor Press, Cold Spring Harbor (NY), 2 edition, 2009.

[13] Richard Beatson, Gjertrud Maurstad, Gianfranco Picco, Appitha Arulappu, Julia Coleman, Hans H. Wandell, Henrik Clausen, Ulla Mandel, Joyce Taylor-Papadimitriou, Marit Sletmoen, and Joy M. Burchell. The breast cancer-associated glycoforms of muc1, muc1-tn and sialyl-tn, are expressed in cosmc wild-type cells and bind the c-type lectin mgl. *PLOS ONE*, 10(5):e0125994, 2015.

[14] Stefan Müller and Franz-Georg Hanisch. Recombinant muc1 probe authentically reflects cell-specific o-glycosylation profiles of endogenous breast cancer mucin: High density and prevalent core 2-based glycosylation. *Journal of Biological Chemistry*, 277(29):26103–26112, 07 2002.

[15] Jerka Dumic, Sanja Dabelic, and Mirna Flögel. Galectin-3: An open-ended story. *Biochimica et Biophysica Acta (BBA) - General Subjects*, 1760(4):616–635, 2006.

[16] D. Nelson and M. Cox. *Lehninger Prinicples of Biochemistry*. W.H. Freeman and Company, 5 edition, 2008.

[17] Avraham Raz and Rcuben Lotan. Endogenous galactoside-binding lectins: a new class of functional tumor cell surface molecules related to metastasis. *Cancer and Metastasis Reviews*, 6(3):433–452, 1987.

[18] Ming Xin, Xin-Wen Dong, and Xiu-Li Guo. Role of the interaction between galectin-3 and cell adhesion molecules in cancer metastasis. *Biomedicine & Pharmacotherapy*, 69:179 – 185, 2015.

[19] Shiro Akahani, Pratima Nangia-Makker, Hidenori Inohara, Hyeong-Reh Choi Kim, and Avraham Raz. Galectin-3: A novel antiapoptotic molecule with a functional bh1 (nwgr) domain of bcl-2 family. *Cancer Research*, 57(23):5272–5276, 1997.

[20] Huei-Min Lin, Bong-Ki Moon, Fei Yu, and Hyeong-Reh Choi Kim. Galectin-3 mediates genistein-induced g2/m arrest and inhibits apoptosis. *Carcinogenesis*, 21(11):1941, 2000.

[21] Hyeong-Reh Choi Kim, Huei-Min Lin, Hector Biliran, and Avraham Raz. Cell cycle arrest and inhibition of anoikis by galectin-3 in human breast epithelial cells. *Cancer Research*, 59(16):4148–4154, 1999.

[22] Karleen M Nicholson and Neil G Anderson. The protein kinase b/akt signalling pathway in human malignancy. *Cellular Signalling*, 14(5):381 – 395, 2002.

[23] S. Ramasamy, S. Duraisamy, S. Barbashov, T. Kawano, S. Kharbanda, and D. Kufe. The muc1 and galectin-3 oncoproteins function in a microrna-dependent regulatory loop. *Mol Cell*, 27:992–1004, 2007.

[24] Yugo Mori, Kaoru Akita, Masakazu Yashiro, Tetsuji Sawada, Kosei Hirakawa, Takeomi Murata, and Hiroshi Nakada. Binding of galectin-3, a β-galactoside-binding lectin, to muc1 protein enhances phosphorylation of extracellular signal-regulated kinase 1/2 (erk1/2) and akt, promoting tumor cell malignancy. *The Journal of Biological Chemistry*, 290(43):26125–26140, 10 2015.

[25] J. Merlin, L. Stechly, S. de Beauce, D. Monte, E. Leteurtre, I. van Seuningen, G. Huet, and P. Pigny. Galectin-3 regulates muc1 and egfr cellular distribution and egfr downstream pathways in pancreatic cancer cells. *Oncogene*, 30(22):2514–2525, 2011.

[26] Lu-Gang Yu, Nigel Andrews, Qicheng Zhao, Daniel McKean, Jennifer F. Williams, Lucy J. Connor, Oleg V. Gerasimenko, John Hilkens, Jun Hirabayashi, Kenichi Kasai, and Jonathan M. Rhodes. Galectin-3 interaction with thomsen-friedenreich disaccharide on cancer-associated muc1 causes increased cancer cell endothelial adhesion. *Journal of Biological Chemistry*, 282(1):773–781, 01 2007.

[27] Qicheng Zhao, Xiuli Guo, Gerard B. Nash, Philip C. Stone, John Hilkens, Jonathan M. Rhodes, and Lu-Gang Yu. Circulating galectin-3 promotes metastasis by modifying muc1 localization on cancer cell surface. *Cancer Research*, 69(17):6799–6806, 2009.

[28] Qicheng Zhao, Monica Barclay, John Hilkens, Xiuli Guo, Hannah Barrow, Jonathan M. Rhodes, and Lu-Gang Yu. Interaction between circulating galectin-3 and cancer-associated muc1 enhances tumour cell homotypic aggregation and prevents anoikis. *Molecular Cancer*, 9:154–154, 2010.

[29] A S Dhillon, S Hagan, O Rath, and W Kolch. Map kinase signalling pathways in cancer. *Oncogene*, 26(22):3279–3290, May 2007.

[30] Jeffrey A. Engelman. Targeting pi3k signalling in cancer: opportunities, challenges and limitations. *Nat Rev Cancer*, 9(8):550–562, 08 2009.

[31] I. V. Safenkova, A. V. Zherdev, and B. B. Dzantiev. Application of atomic force microscopy for characteristics of single intermolecular interactions. *Biochemistry (Moscow)*, 77(13):1536–1552, 2012.

[32] Shaoyang Liu and Yifen Wang. Application of afm in microbiology: a review. *Scanning*, 32(2):61–73, 3 2010.

[33] Greg Haugstad. *Atomic Force Microscopy*. Wiley, Somerset, UNITED STATES, 2012.

[34] Peter Schön. Imaging and force probing rna by atomic force microscopy. *Methods*, 103:25–33, 7 2016.

[35] Marit Sletmoen, Catharina Davies, Katarzyna Psonka-Antonczyk, and Bjørn Stokke. Light and force based molecular imaging. Lecture notes for PhD course, 2011.

[36] BRUKER. *NanoScope Analysis1.50 User Manual*.

[37] Evan Evans. Looking inside molecular bonds at biological interfaces with dynamic force spectroscopy. *Biophysical Chemistry*, 82(2–3):83–97, 1999.

[38] Peter Hinterdorfer and Ziv Reich. *Molecular Recognition Force Microscopy: From Simple Bonds to Complex Energy Landscapes*, pages 279–308. Springer Berlin Heidelberg, Berlin, Heidelberg, 2008.

[39] Xi Zhang, Chuanjun Liu, and Zhiqiang Wang. Force spectroscopy of polymers: Studying on intramolecular and intermolecular interactions in single molecular level. *Polymer*, 49(16):3353 – 3361, 2008.

[40] A. Gunning, Devon Kavanaugh, Elizabeth Thursby, Sabrina Etzold, Donald MacKenzie, and Nathalie Juge. Use of atomic force microscopy to study the multi-modular interaction of bacterial adhesins to mucins. *International Journal of Molecular Sciences*, 17(11):1854, 2016.

[41] Keir C. Neuman and Attila Nagy. Single-molecule force spectroscopy: optical tweezers, magnetic tweezers and atomic force microscopy. *Nat Meth*, 5(6):491–505, 2008.

[42] William J. Greenleaf, Michael T. Woodside, and Steven M. Block. High-resolution, single-molecule measurements of biomolecular motion. *Annual review of biophysics and biomolecular structure*, 36:171–190, 2007.

[43] Kristin E Haugstad, Bjørn T Stokke, C Fred Brewer, Thomas A Gerken, and Marit Sletmoen. Single molecule study of heterotypic interactions between mucins possessing the tn cancer antigen. *Glycobiology*, 25(5):524–534, 2015.

[44] Armend Gazmeno Håti, Finn Lillelund Aachmann, Bjørn Torger Stokke, Gudmund Skjåk Bræk, Gudmundk Braek, and Marit Sletmoen. Energy landscape of alginate-epimerase interactions assessed by optical tweezers and atomic force microscopy. -, 2015.

[45] Emrah Celik and Vincent T. Moy. Nonspecific interactions in afm force spectroscopy measurements. *Journal of Molecular Recognition*, 25(1):53–56, 2012.

[46] Evan Evans. Introductory lecture energy landscapes of biomolecular adhesion and receptor anchoring at interfaces explored with dynamic force spectroscopy. *Faraday Discussions*, 111(0):1–16, 1999.

[47] E. Evans and K. Ritchie. Dynamic strength of molecular adhesion bonds. *Biophysical Journal*, 72(4):1541–1555, 1997.

[48] Anna Rita Bizzarri and Salvatore Cannistraro. The application of atomic force spectroscopy to the study of biological complexes undergoing a biorecognition process. *Chemical Society Reviews*, 39(2):734–749, 2010.

[49] Olga K. Dudko, Jérôme Mathé, Attila Szabo, Amit Meller, and Gerhard Hummer. Extracting kinetics from single-molecule force spectroscopy: Nanopore unzipping of dna hairpins. *Biophysical Journal*, 92(12):4188–4195, 2007.

[50] Olga K. Dudko, Gerhard Hummer, and Attila Szabo. Theory, analysis, and interpretation of single-molecule force spectroscopy experiments. *Proceedings of the National Academy of Sciences*, 105(41):15755–15760, 2008.

[51] Raymond W. Friddle, Aleksandr Noy, and James J. De Yoreo. Interpreting the widespread nonlinear force spectra of intermolecular bonds. *Proceedings of the National Academy of Sciences*, 109(34):13573–13578, 08 2012.

[52] Anna Rita Bizzarri and Salvatore Cannistraro. Antigen–antibody biorecognition events as discriminated by noise analysis of force spectroscopy curves. *Nanotechnology*, 25(33):335102, 2014.

[53] Malin Bäckström, Thomas Link, Fredrik J. Olson, Hasse Karlsson, Rosalind Graham, Gianfranco Picco, Joy Burchell, Joyce Taylor-Papadimitriou, Thomas Noll, and Gunnar C. Hansson. Recombinant muc1 mucin with a breast cancer-like o-glycosylation produced in large amounts in chinese-hamster ovary cells. *Biochemical Journal*, 376(3):677–686, 2003.

[54] Marit Sletmoen, Tarun K. Dam, Thomas A. Gerken, Bjørn T. Stokke, and Curtis Fred Brewer. Single-molecule pair studies of the interactions of the α-galnac (tn-antigen) form of porcine submaxillary mucin with soybean agglutinin. *Biopolymers*, 91(9):719–728, 2009.

[55] Marit Sletmoen and Bjørn T. Stokke. Single-molecular pair unbinding studies of mannuronan c-5 epimerase alge4 and its polymer substrate. *Biomacromolecules*, 5(4):1288–1295, 2004.

[56] Maria J. Marcos, Rosana Chehin, Jose L. Arrondo, Galina G. Zhadan, Enrique Villar, and Valery L. Shnyrov. ph-dependent thermal transitions of lentil lectin. *{FEBS} Letters*, 443(2):192 – 196, 1999.

[57] Fahad M. Almutairi, Jose-Gines Hernandez Cifre, Gary G. Adams, M. Samil Kök, Alan R. Mackie, Jose Garcia de la Torre, and Stephen E. Harding. Application of recent advances in hydrodynamic methods for characterising mucins in solution. *European Biophysics Journal*, 45(1):45–54, 2016.

[58] A.N. Round, M. Berry, T.J. McMaster, S. Stoll, D. Gowers, A.P. Corfield, and M.J. Miles. Heterogeneity and persistence length in human ocular mucins. *Biophysical Journal*, 83(3):1661 – 1670, 2002.

[59] Bruno Zappone, Navinkumar J. Patil, Jan B. Madsen, Kirsi I. Pakkanen, and Seunghwan Lee. Molecular structure and equilibrium forces of bovine submaxillary mucin adsorbed at a solid–liquid interface. *Langmuir*, 31(15):4524–4533, 2015. PMID: 25806669.

[60] Randal Shogren, Thomas A. Gerken, and Neil Jentoft. Role of glycosylation on the conformation and chain dimensions of o-linked glycoproteins: light-scattering studies of ovine submaxillary mucin. *Biochemistry*, 28(13):5525–5536, 1989. PMID: 2775721.

[61] Harold P Erickson. Size and shape of protein molecules at the nanometer level determined by sedimentation, gel filtration, and electron microscopy. *Biological Procedures Online*, 11:32–51, 2009.

[62] Michel Grandbois, Martin Beyer, Matthias Rief, Hauke Clausen-Schaumann, and Hermann E. Gaub. How strong is a covalent bond? *Science*, 283(5408):1727–1730, 1999.

[63] Todd A. Sulchek, Raymond W. Friddle, Kevin Langry, Edmond Y. Lau, Huguette Albrecht, Timothy V. Ratto, Sally J. DeNardo, Michael E. Colvin, and Aleksandr Noy. Dynamic force spectroscopy of parallel individual mucin1–antibody bonds. *Proceedings of the National Academy of Sciences of the United States of America*, 102(46):16638–16643, 2005.

[64] Chih-Kung Lee, Yu-Ming Wang, Long-Sun Huang, and Shiming Lin. Atomic force microscopy: Determination of unbinding force, off rate and energy barrier for protein–ligand interaction. *Micron*, 38(5):446–461, 2007.

Appendix A

Dynamic force spectroscopy analysis

A.1 MUC1-T - Gal3 interaction, histograms

Histograms obtained from subgroups of increasing loading rate, from scatterplot of force versus loading rate of interactions between MUC1-T and Gal3 obtained by AFM, presented in Figure 3.4.1. Presented with a constrained fit of Equation 1.6.8.

A.2 MUC1-ST - Gal3 interaction, histograms

Histograms obtained from subgroups of increasing loading rate, from scatterplot of force versus loading rate of interactions between MUC1-ST and Gal3 obtained by AFM, presented in Figure 3.5.1. Presented with a constrained fit of Equation 1.6.8.

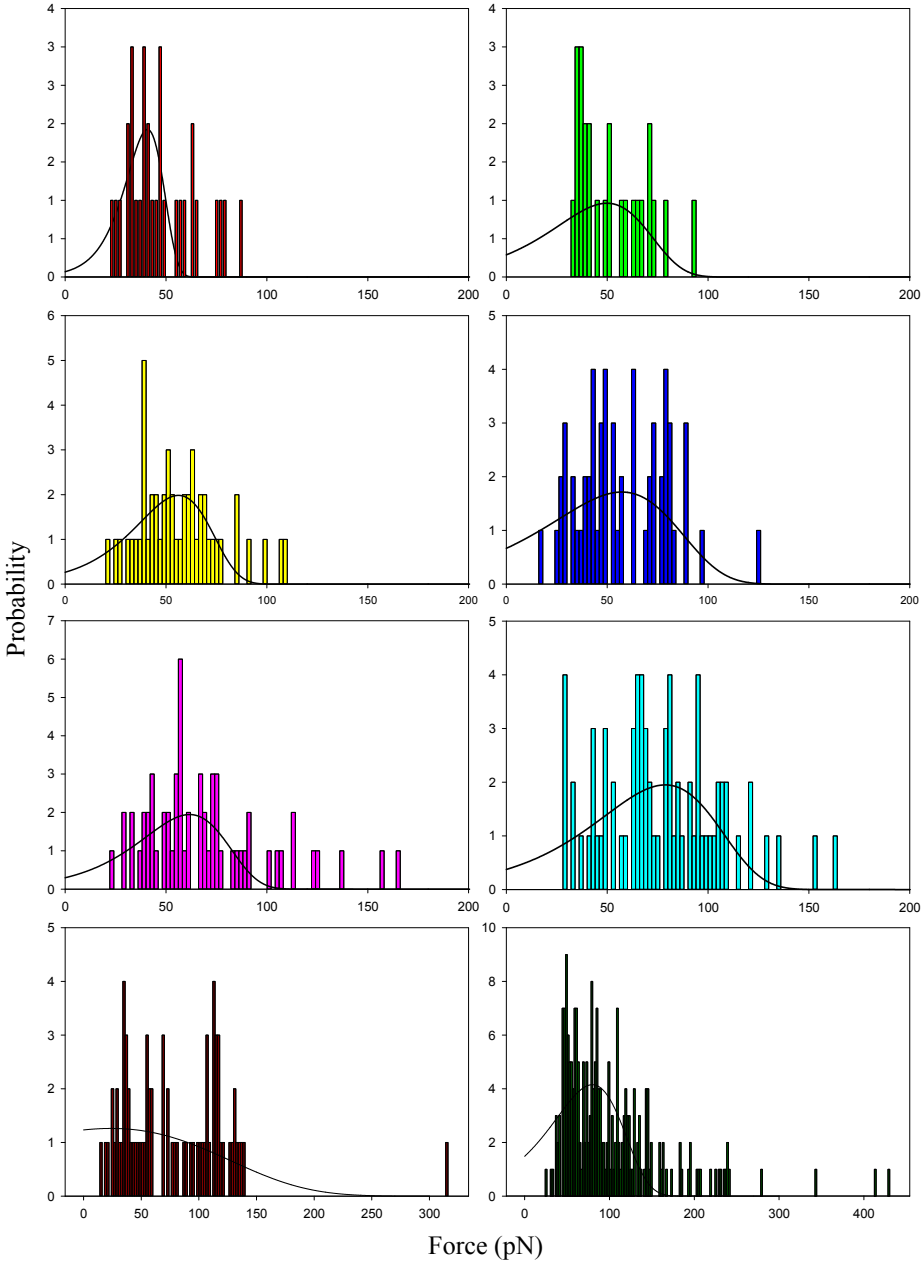

Figure A.1.1: Histograms obtained from the scatterplot presented in Figure 3.4.1 of force versus loading rate obtained by AFM for interactions between MUC1-T and Gal3, each presented with a constrained fit of Equation 1.6.8

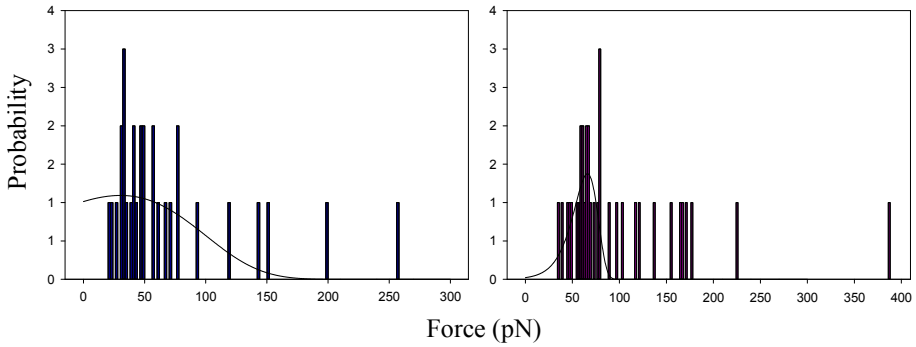

Figure A.1.2: Histograms obtained from the scatterplot presented in Figure 3.4.1 of force versus loading rate obtained by AFM for interactions between MUC1-T and Gal3, each presented with a constrained fit of Equation 1.6.8

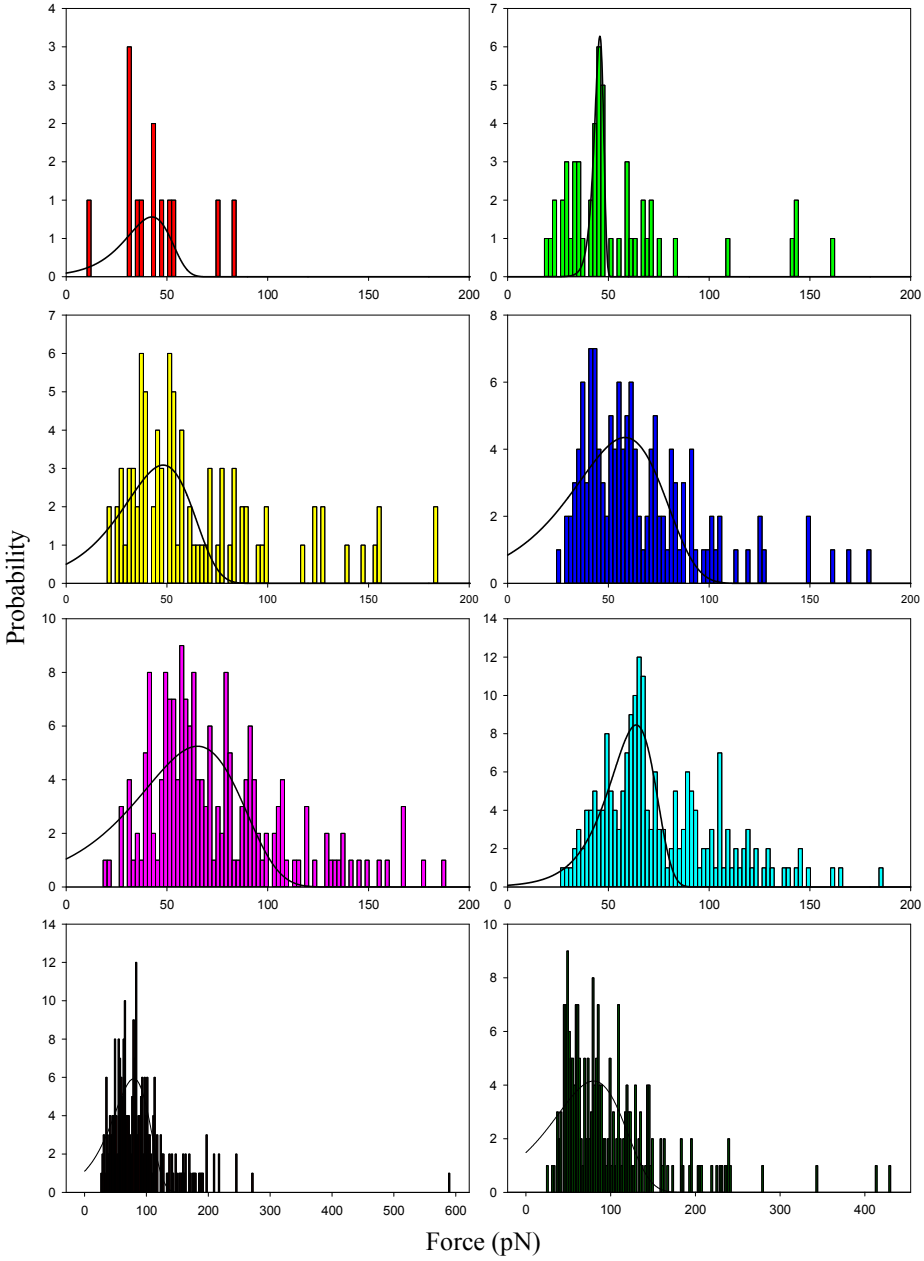

Figure A.2.1: Histograms obtained from the scatterplot presented in Figure 3.4.1 of force versus loading rate obtained by AFM for interactions between MUC1-T and Gal3, each presented with a constrained fit of Equation 1.6.8

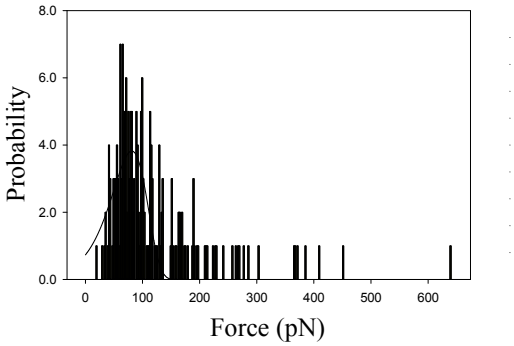

Figure A.2.2: Histograms obtained from the scatterplot presented in Figure 3.4.1 of force versus loading rate obtained by AFM for interactions between MUC1-T and Gal3, each presented with a constrained fit of Equation 1.6.8

Appendix B

Result from linear regression on DFS with OT and AFM data

Result of a linear regression performed on Figure 4.4.1 by the use of SigmaPlot.

Plot 5

Order 1

All curves:

Coefficients:

b[0]	-35,9457068585
b[1]	27,5667795607
r^2	0,9511221338

Function values:

x	f(x)
1,591064607	7,9148204303
1,6411898496	9,2966119427
1,6913150922	10,6784034552
1,7414403347	12,0601949676
1,7915655773	13,4419864801
1,8416908199	14,8237779926
1,8918160625	16,205569505
1,941941305	17,5873610175
1,9920665476	18,9691525299
2,0421917902	20,3509440424
2,0923170328	21,7327355548
2,1424422753	23,1145270673
2,1925675179	24,4963185798
2,2426927605	25,8781100922
2,2928180031	27,2599016047
2,3429432456	28,6416931171
2,3930684882	30,0234846296
2,4431937308	31,405276142
2,4933189734	32,7870676545
2,5434442159	34,168859167
2,5935694585	35,5506506794
2,6436947011	36,9324421919
2,6938199436	38,3142337043
2,7439451862	39,6960252168
2,7940704288	41,0778167293
2,8441956714	42,4596082417
2,8943209139	43,8413997542
2,9444461565	45,2231912666

2,9945713991	46,6049827791
3,0446966417	47,9867742915
3,0948218842	49,368565804
3,1449471268	50,7503573165
3,1950723694	52,1321488289
3,245197612	53,5139403414
3,2953228545	54,8957318538
3,3454480971	56,2775233663
3,3955733397	57,6593148788
3,4456985823	59,0411063912
3,4958238248	60,4228979037
3,5459490674	61,8046894161
3,59607431	63,1864809286
3,6461995526	64,568272441
3,6963247951	65,9500639535
3,7464500377	67,331855466
3,7965752803	68,7136469784
3,8467005228	70,0954384909
3,8968257654	71,4772300033
3,946951008	72,8590215158
3,9970762506	74,2408130283
4,0472014931	75,6226045407
4,0973267357	77,0043960532